TITIN CONTRIBUTION TO ACTIVE MUSCLE

By Siwoo Jeong

A Dissertation

Submitted in Partial Fulfillment

of the Requirements for the Degree of

Doctor of Philosophy

in Bioengineering

Northern Arizona University

January 2022

Approved:

Kiisa C. Nishikawa, Ph.D., Chair

Monica A. Daley, Ph.D.

Stan L. Lindstedt, Ph.D.

Timothy A. Becker, Ph.D.

ABSTRACT

TITIN CONTRIBUTION TO ACTIVE MUSCLE

SIWOO JEONG

The aim of this dissertation is to compare the traditional ‘muscle as motor’ viewpoint to the alternative viewpoint ‘muscle as composite material’. We make three parts to achieve the aim. We first investigate whether the contribution of activation and length perturbation on muscle force depends on length history. The effect of length history is to alter muscle stiffness. The alteration of muscle stiffness determines the role of activation and length perturbation in determining muscle force. That is, muscle responds to activation and length perturbation depending on length history. Muscle models based on the ‘muscle as motor’ viewpoint fail to predict muscle force accurately under dynamic conditions in part because they cannot account for the history dependence of muscle force. An alternative muscle viewpoint should be able to explain the history dependent muscle force to enlarge our knowledge about how muscle works under dynamic conditions.

In the second part, we focus on the ratio of muscle force to stiffness. The ratio of force to stiffness has been believed to be relatively constant during isometric contraction because both isometric force and stiffness are linearly related to the number of formed cross-bridge. However, the ratio depends on shortening velocity as well as is not constant during the isometric force redevelopment period following active shortening. This finding invokes ‘stress-induced inhibition’ where weakly-bound cross bridge generated by active shortening contributes only to stiffness with no contribution to force. The weakly-bound cross bridge is

able to explain non-zero y-intercepts of the relationship between force and stiffness, but not the lower slope for the slower velocity. In the ‘stress-induced inhibition’, the slower shortening velocity should distort actin more due to the bigger stress. The more distorted actin induces the bigger number of weakly-bound cross bridge, which should result in the bigger slope of the relationship between force and stiffness. This is not compatible with our results. Another possible explanation of the finding is a change in titin stiffness. According to the winding filament hypothesis, titin equilibrium length is modulated by cross-bridge force. Active shortening at different velocity could generate the different initial conditions for titin strain and equilibrium position, and then titin differently responds to an increase in cross bridge force depending on the initial conditions. The tunable titin stiffness contributes to the variable muscle stiffness.

Finally, this dissertation develops a titin-clutch model based on a composite material viewpoint. The titin-clutch model predicts frequency-dependent muscle force better than the Hill model. The model has three subunits: a contractile, titin, and series elastic element. The pulley connects the titin to the contractile element in series and parallel. The history-dependent pulley position implements the history-dependent contributions of length perturbation and activation to force. When the contractile force increases, pulley rotates counterclockwise direction, then titin element wraps around a pulley. The interaction between them regulates titin stiffness. The dissertation concludes that incorporating a tunable titin spring in muscle models improves the predictions of muscle force under dynamic conditions.

Preface

The works comprising this dissertation are taken from papers that are planned to be submitted soon in collaboration with other authors. The present author is the primary author of all works and performed majority of the data collection and analysis and development of the simulation model. Dr. Nishikawa provided overall guidance of all projects. Dr. Sponberg provided *in situ* data to validate muscle models in Chapter 4.

Table of Contents

List of Tables

List of Figures

Acknowledgement

I would like to thank my supervisor, Kiisa Nishikawa. The completion of this dissertation could not have been possible without her guidance and mentoring during my Ph.D. course.

I am very grateful to my family members: Juok Kang and Jiu Jeong. I also would like to thank my parents, Jongsaeng Jeong, Soonboon Lee, and Taejung Kang for their continuous support.

Chapter 1. Introduction

Research on the mechanisms of muscle contraction has traditionally been conducted from the perspective that muscles function as a motors in that neural activation acts like a voltage to generate actuator force (Brenner and Eisenberg, 1986; Davies et al., 1967). The traditional perspective has been motivated by the process of muscle shortening contraction (Hill, 1938; Huxley, 1957; Huxley and Niedergerke, 1954). When electrical signals arrive at muscle, calcium is released and binds to troponin so that tropomyosin can slide away from the binding sites on the actin filament. This allows the myosin heads to bind to these exposed binding sites and form cross bridges. The cross bridges then pull the actin filament toward the center of the sarcomere. Because each cross bridge can pull only a short distance (up to 11 nm, Brunello et al., 2014; Dominguez et al., 1998; Geeves and Holmes, 2005; Rayment et al., 1993), a repetitive process including detachment, pre-power stroke, attachment, and power stroke is required to produce force, and this process requires energy (Geeves and Holmes, 2005; Lymn and Taylor, 1971). In this process, the cross bridge is the fundamental unit to produce muscle force (Huxley, 1957).

The magnitude of force has been thought to reflect the number of attached cross bridges (Gordon et al., 1966; Huxley, 1957). One factor that determines the number of attached cross-bridge is the level of activation. The amplitude of activation is correlated with isometric muscle force (Alkner et al., 2000; Hof and van den Berg, 1977; Hylander and Johnson, 1989), so it is assumed that the number of attached cross-bridge increases with the amplitude of activation. Another factor that influences muscle force is muscle length. According to the

sliding filament theory, the overlap width between the myosin and actin filaments is proportional to the number of attached cross bridges (Gordon et al., 1966). The overlap width is determined by muscle length. The rate of change in muscle length alters both the force per cross bridge and the number of attached cross-bridges in the two-state cross-bridge model (Huxley, 1957). A spring force placed between the myosin head and the binding site on actin represents the force of each cross bridge. When muscle is lengthened, extension of the spring produces the greater force, but when muscle is shortened, the spring force should decrease. In addition, a longer sarcomere has a higher rate of cross-bridge attachment based on the rate function derived from the force velocity relationship (Hill, 1938). In summary, muscle force is assumed to be proportional to the number of attached cross bridges and the force produced by each cross-bridge force determined by the level of activation, muscle length and the rate of change in muscle length.

In the traditional muscle viewpoint, force should be determined by a muscle's current activation, length, and velocity. However, muscle force is also affected by length history. For example, isometric force following active lengthening is greater than the isometric force given the same length and activation (Abbott and Aubert, 1952; Edman et al., 1982; Herzog et al., 2016; Nishikawa, 2016). Conversely, active shortening before isometric contraction decreases the force compared to the purely isometric force (Abbott and Aubert, 1952; De Ruiter et al., 1998; Herzog and Leonard, 1997; Tahir et al., 2020). In activities of daily living, muscles undergo large variations in strain up to 40% of their resting length (Daley and Biewener, 2011). To understand human and animal movement and to accurately predict muscle force, the history dependence of muscle force must be taken into account (Seiberl et al., 2013).

Previous studies suggested that the history-dependence of muscle force can be

explained within the cross-bridge theory with no additional components (Morgan, 1990; Morgan et al., 2000). In the force-length relationship, the descending limb shows negative stiffness which usually implies instability (Gordon et al., 1966; Zahalak, 1997). The instability induces sarcomere non-uniformity in muscle after active lengthening (Morgan, 1990; Morgan et al., 2000). On the descending limb of the force length relationship, shorter sarcomeres produce greater force than longer sarcomeres. The shorter sarcomeres pull the neighbors to longer lengths until the passive force of the longer sarcomere is the same as the force of the shorter sarcomere. Therefore, compared to a muscle with no length non-uniformity, a muscle with non-uniform sarcomeres can produce greater isometric force at the same length (Morgan, 1990; Morgan et al., 2000).

Although the sarcomere non-uniformity may explain the history-dependence of muscle force with no additional elements (Morgan, 1990; Morgan et al., 2000), several studies have enumerated observations which the sarcomere non-uniformity cannot explain (Johnston et al., 2016; Lee and Herzog, 2008; Leonard et al., 2010; Rassier et al., 2003). The increase in force due to sarcomere non-uniformity can occur only on the descending limb of the force-length relationship, because unlike the descending limb the longer sarcomere produces greater force on the ascending limb. During isometric contraction, the longer sarcomere producing the greater force must be shortened by pulling its neighbor shorter sarcomeres. These interactions remove the non-uniformity, so that all sarcomeres should produce the same force at the same length. In other words, if the history-dependence of muscle force were due to sarcomere non-uniformity, then residual force enhancement should not be observed on the ascending limb. However, numerous studies have shown residual force enhancement on the ascending limb of the force-length relationship in fibers (Peterson et al., 2004; Sugi, 1972), muscles *in situ* (Cook

and McDonagh, 1995; Herzog and Leonard, 2002; Lee and Herzog, 2002), and myofibrils (Pun et al., 2010). Additionally, the sarcomere non-uniformity describes interactions of neighboring sarcomeres to maintain the force balance. Thus, if sarcomere inhomogeneity were the only mechanism, then a single sarcomere should not be able to produce a history-dependent force. However, force enhancement has been observed in a single sarcomere preparation (Leonard et al., 2010; Rassier et al., 2003). These findings suggest that alternative mechanisms are required to explain the history-dependence of muscle force.

Titin is a giant protein that spans from the Z-disk to the M-line in the sarcomere (Furst et al., 1988; Itoh et al., 1988; Wang et al., 1991). In the A-band of muscle sarcomeres, titin attaches to myosin, whereas I-band titin extends like a spring (Li et al., 1995; Linke et al., 1997; Wang et al., 1993). I-band titin has been demonstrated to maintain sarcomere integrity as a primary contributor to passive force (Horowits and Podolsky, 1987; Linke et al., 1998a). Recently, it has been suggested that I-band titin contributes to active force as well as passive force by increasing its stiffness in the presence of Ca^{2+} (Dutta et al., 2018).

The N2A region of titin binds to actin in the presence of Ca^{2+}, which makes titin shorter and stiffer by removing the compliant Ig domains (Dutta et al., 2018). Muscle length at the onset of activation should determine the distance between the Z-disc and the binding site on actin for N2A titin (Gautel and Goulding, 1996; Linke et al., 1998a; Linke et al., 1998b; Nishikawa, 2016). If muscle length at the onset of activation is different, the strain of the free titin segment should be different even during isometric contraction at same length due to the different binding site on actin. Because titin is in parallel with cross bridges (Herzog, 2018; Nishikawa, 2016; Nishikawa, 2020), changes in titin strain will change titin force and thereby influence muscle force. The amount of residual force enhancement increases when the initial

isometric contraction length is shorter (Bullimore et al., 2007; Edman et al., 1978; Edman et al., 1982; Hisey et al., 2009). This observation supports a role for titin-actin binding in determining muscle force.

Due to their simplicity (Lloyd and Besier, 2003), Hill-type muscle models are commonly used to estimate muscle force. These simple models estimate muscle force in accordance with the traditional muscle viewpoint of muscle as motor (Lloyd and Besier, 2003; Zajac, 1989). Maximal isometric force indicates the force capacity, and muscle length and the rate of change in length determine muscle force for a given level of activation (Dick et al., 2017; Lee et al., 2013; Wakeling et al., 2021). Although these models have the advantage of being relatively simple, the accuracy of their force predictions is relatively low. Previous research demonstrates the inaccuracy of Hill-type muscle models under dynamic conditions. Hill-type models yielded low r^2 values for human medial gastrocnemius during cycling (r^2 = 0.54; Dick et al., 2017) and for goat medial gastrocnemius during walking, galloping, and trotting ($r^2 < 0.51$; Lee et al., 2013). Considering that dynamics of muscle length and activation is complex during *in vivo* movement, the inability of the Hill models to predict the history-dependence of muscle force results in low accuracy of force predictions. However, Hill-type muscle models fail to explain the length-dependence of activation dynamics (Shue and Crago, 1998) and the history-dependence of force (Perreault et al., 2003; Sandercock and Heckman, 1997; Scovil and Ronsky, 2006).

To overcome these limitations of Hill-type muscle models, new muscle models that include history-dependence of force are required. An alternative to the “muscle as motor” paradigm is the viewpoint that muscle is an active composite material with tunable viscoelastic properties (Nishikawa, 2020). Composite materials which have two or more constituent

materials exhibit their own mechanical behaviors, referred as viscoelasticity, depending on the properties of the constituent materials. When muscle is considered as a composite material, force is determined not only by activation but also by the response to deformation by applied forces. Activities of daily living require repetitively adjustments to unexpected length perturbation by external forces. For example, during locomotion on uneven terrain, leg muscles must be adjusted their force to maintain balance or to prevent falling despite variations in terrain (Daley and Biewener, 2011; Daley et al., 2009). Because not all perturbations can be anticipated in advance, and because reflex loops incur inevitable delays that can result in instability, the intrinsic dynamics of muscle viscoelastic properties is important for modulation the force response to perturbations. From the composite material viewpoint, the role of activation is to tune the viscoelastic properties of muscle so that the response to deformation by unpredictable external forces results in adaptive control of movement (Nishikawa et al., 2007; Nishikawa et al., 2013).

In this study, I will evaluate the hypothesis that muscle is an active composite material using different experiments and simulations. First, I will test whether muscle force can be decoupled from activation. How muscle force responds to time varying activation under dynamic conditions will be evaluated. In “composite material” muscle, activation will have a large effect on muscle force at relatively slow velocity but not at fast velocity. Second, I will investigate which sarcomeric elements affect muscle intrinsic viscoelastic properties. To infer what causes the viscoelastic properties of muscle to change, I will determine the ratio of muscle force to stiffness as a function of active shortening. Following the cross-bridge theory, the ratio should be constant during isometric contraction. If the ratio is not constant, elements in addition to cross bridge would be required to explain the non-constant ratio. The results will provide

insights into the role of additional elastic elements in active muscle. Finally, based on the research results, I will modify the previously established titin-clutch model, validate, and test the model using *in situ* data from cockroach leg muscles during length perturbations.

Chapter 2. Decoupling between muscle force and activation

2.1 Background

The role of activation in determining muscle force depends on muscle length (Shue and Crago, 1998). Muscles continuously adjust to unexpected perturbations during locomotion on uneven terrain, performing various roles as motors, springs, and brakes (Ahn et al., 2006; Daley and Biewener, 2003; Dickinson et al., 2000; Roberts et al., 1997). The phase of activation shifts the mechanical role of muscles by influencing the shape and magnitude of force. Conversely, muscle length trajectories affect the role of activation in determining muscle force (Sandercock and Heckman, 1997). Since most daily activities are performed in unsteady or perturbed conditions, understanding how the role of activation depends on perturbations is important for understanding how muscle force is controlled.

From the traditional viewpoint of 'muscle as a motor', force is a consequence of activation (Brenner and Eisenberg, 1986; Davies et al., 1967). The phase of activation determines the onset, duration, and end of muscle force as well as the magnitude of activation is proportional to the amplitude of force (Lloyd and Besier, 2003; Zajac, 1989). However, it is unlikely that activation alone controls muscle force during natural movements (Nishikawa et al., 2013). For example, activation alone cannot control leg or foot movements to stabilize unexpected perturbations during locomotion (Dudek and Full, 2006; Full et al., 1998). Therefore, the 'muscle as a motor' viewpoint could only apply to steady-state isometric contractions.

Recent studies of muscle dynamics suggest that muscle force may be decoupled from activation via effects of muscle length perturbations (Daley, 2018; Daley and Biewener, 2011;

Daley et al., 2009; Lappin et al., 2006; Libby et al., 2020; Robertson and Sawicki, 2015; Sponberg et al., 2011b). In studies of a leg muscle in the cockroach, the mechanical response of the muscle differed depending on the motor task, such as standing or running, despite similar activation (Sponberg et al., 2011a). In a work-loop experiment, the shape of a work-loop is sensitive to small changes in velocity (Robertson and Sawicki, 2015). Furthermore, isometric force following active lengthening is higher (Abbott and Aubert, 1952; Edman et al., 1982; Herzog et al., 2016; Nishikawa, 2016) and isometric force following shortening is lower (Abbott and Aubert, 1952; De Ruiter et al., 1998; Herzog and Leonard, 1997; Lee and Herzog, 2003; Tahir et al., 2020) than the purely isometric force at the same final length and activation. These findings support the hypothesis that muscle force in dynamic conditions cannot be explained solely by activation.

Previous studies of *in vivo* length-force dynamics in guinea fowl during running over potholes and obstacles have shown that length perturbations are associated with peak muscle force (Daley and Biewener, 2011; Daley et al., 2009). The lateral gastrocnemius muscle undergoes length perturbations during stance, following active shortening. Uneven terrains such as obstacles and potholes caused the phase of length perturbations to differ from level running, which resulted in variable peak force. When length perturbation occurred earlier on stepping up, peak muscle force increased, however the late phase of length perturbation on stepping down resulted in lower peak force. Of course, there was a change in electromyography (EMG) intensity between level walks and obstacle strides. As stepping up, EMG intensity increased, but when stepping down, EMG intensity was not different from at the level walk. That is, EMG intensity was not able to entirely explain the variable peak force. In these findings, the role of activation in muscle force is no longer to instruct a muscle's force-time trajectory

under dynamic conditions, rather the phase of length perturbation appears to play an important role in determining muscle force. Critically, activation does not contain information about the timing or magnitude of muscle force under dynamic conditions.

Muscle force during length perturbations can be increased or decreased by length history, despite same activation (Libby et al., 2020). The result suggests that the relative contribution of length perturbation and activation to muscle force is modulated by length history, length history determines preload. Preload refers to force at the onset of length perturbation. Because muscle force is linearly correlated with muscle stiffness (Kirsch et al., 1994), preload determines muscle stiffness. If the effect of length history is to change muscle stiffness, then the contribution of length perturbation or activation to muscle force may depend on tunable stiffness.

To investigate the effects of muscle stiffness on the relative contributions of activation and length perturbations to muscle force, we designed an experiment in which muscles first develop force isometrically and are shortened at different velocities to induce different muscle stiffness. According to the force-velocity relationship, when shortening velocity increases, both muscle force and stiffness decrease. During active shortening, time-varying activation was used to measure how much muscle force reflects the time-varying activation amplitude. Additionally, we controlled the amplitude of length perturbations and measured the force response of muscles. Finally, we investigated the inter-relationships among muscle force, length perturbations, and activation in a series of experiments in which muscle stiffness was controlled by changing the muscle shortening velocity.

2.2 Methods

2.2.1 Animals

Mice of the strain B6C3Fe a/a-Ttn^{mdm}/J were obtained from the Jackson Laboratory (Bar Harbor, ME, USA) and a breeding colony was established in the animal care facility at Northern Arizona University (NAU). Soleus muscles from homozygous wild-type mice (n = 12; female = 6; male = 6; mass = 34.3 ± 6.7g) were used in this study. The institutional Animal Care and Use Committee at NAU approved the experimental protocol and use of animals.

2.2.2 Muscle preparation

Wild-type mice were sacrificed by isoflurane overdose (1-2% isoflurane mixed with oxygen) confirmed by cervical dislocation. Soleus muscles were isolated from the hindlimb and immersed in a mammalian Krebs-Ringer bath (in mmol l^{-1}: 137 NaCl, 5 KCl, 1 $MgSO_4$, 1 24 $NaHCO_3$, 1 NaH_2PO_4, 11 dextrose, 2 $CaCl_2$, pH 7.2 at room temperature) with 95% O_2 and 5% CO_2. Soleus muscles were attached to a dual servomotor force lever (Aurora Scientific, Inc., Series 300B, Aurora, ON, Canada) at one end and an inflexible hook at the other end. The servomotor controlled muscle length and measured position and force.

All soleus muscles were stimulated using an electrical field generated between two platinum electrodes connected to a Grass S48 stimulator. In order to determine optimal muscle length (L_0), muscles were fully activated using square wave pulses at 60V and 75Hz, and muscle length was adjusted until maximum isometric muscle force (P_0) was established. At the end of the experiments, P_0 was measured to ensure that P_0 was maintained throughout the experiments. Muscles used in the analysis experienced < 15% drop in force during an experiment.

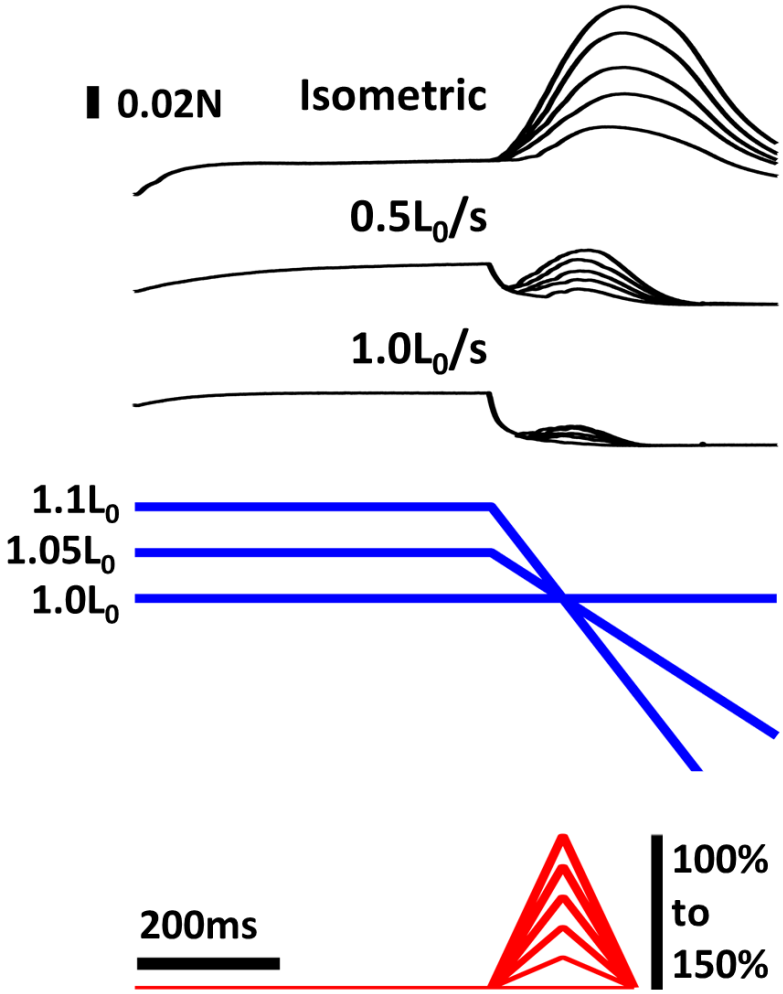

Figure 2.1: Methods for Protocol 1 to evaluate the effect of active shortening on muscle force response to amplitude of activation. Muscles reached submaximal steady-state force at three different lengths ($1.10L_0$, $1.05L_0$ and $1.0L_0$), and then were actively shortened at $1.0L_0$/s, $0.5L_0$/s or held isometrically (force, black; length, blue). When muscles started shortening actively, the amplitude of activation increased until muscle length reached L_0 (activation, red). Six different peak amplitudes of activation were performed: 100%, 110%, 120%, 130%, 140% and 150% of the amplitude of activation during the first submaximal isometric contraction (~7.0% P_0).

2.2.3 Experimental protocols

Our hypotheses in this study were that: 1) active shortening reduces muscle stiffness; 2) the reduced stiffness decreases the relative contribution of activation to muscle force; and 3)

the response of muscle to length perturbations is affected by the muscle stiffness. Two protocols were performed to test those hypotheses. The protocols evaluated effects of active shortening on muscle stiffness, as well as the effects of muscle stiffness on the response to activation (protocol 1) or length perturbations (protocol 2).

Protocol 1 measured how the response of muscle force to time-varying activation depends on muscle stiffness. Muscles were stimulated isometrically at submaximal voltage (give value) and frequency (give value) until they until they reached a steady-state force of 7.0 ± 3.0% P_0 in ~ 0.7s. Once isometric force reached steady state, active shortening was performed at two velocities (1.0 L_0/s, 0.5 L_0/s) and under isometric conditions. At the midpoint of active shortening, muscle length was held constant at L_0 by changing the starting length (Fig. 2.1, blue). To evaluate how muscle force depends on the amplitude of activation, the amplitude of activation during active shortening was varied using an A-M Systems Model 4100 stimulator (A-M Systems, Carlsborg, Washington, USA).

In protocol 1, activation started increasing at the onset of active shortening. The amplitude of activation increased linearly for 100ms, and then decreased linearly for 100ms (Fig. 2.1, red). Peak activation occurred at the midpoint of active shortening, which also occurred at muscle optimal length (L_0). Six different activation amplitudes were used: 100%, 110%, 120%, 130%, 140% and 150% of the amplitude for the first submaximal isometric contraction generated by square wave pulses at 3.87 ± 0.88V and 75Hz. To measure instantaneous muscle stiffness, quick length transients (0.9% L_0 at a speed of 3L_0/s) were performed at L_0 during active shortening.

In protocol 2, the response of muscle force to length perturbations was measured for different values of muscle stiffness, established by varying the shortening velocity. As in protocol 1, isometric contraction and active shortening at 1.0 and 0.5 L_0/s were performed (Fig.

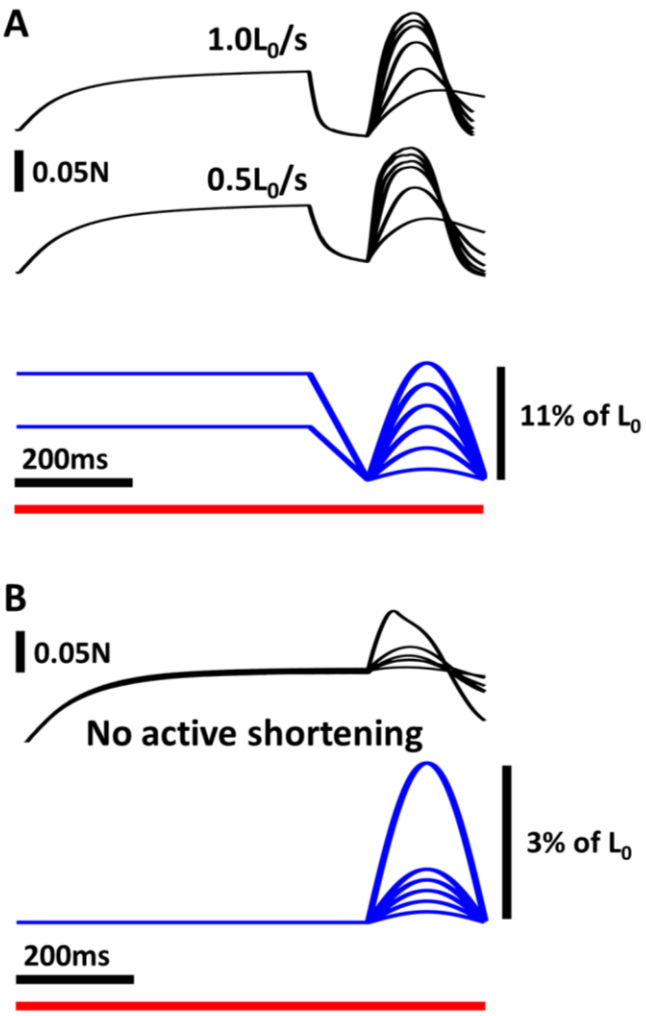

Figure 2.2: Methods for Protocol 2 to evaluate the effect of active shortening on the response of muscle force to length perturbations at the same length and activation. Muscle force (black), length (blue) and activation (red). **A)** Active shortening was performed from $1.1L_0$ to $1.0L_0$ (above) and from $1.05L_0$ to $1.0L_0$ (below) at $1.0L_0$/s and $0.5L_0$/s, respectively. After active shortening, length perturbations were performed at L_0. The amplitudes of the length perturbations were 1, 3, 5, 7, 9 and 11% L_0. **B)** The muscles developed force isometrically at L_0 and then length perturbations were performed at six different amplitudes: 0.2, 0.4, 0.6, 0.8, 1 and 3% of L_0. The level of activation was constant at ~35% P_0 throughout the trials.

2.2, blue). At the midpoint of active shortening where muscle length is L_0 in all trials, length perturbations were performed. The shape of the length perturbation was varied based on a half sinusoidal curve at a frequency of 2.5 Hz. We used two different sets of the amplitude of the length perturbation for the trials with no active shortening and the trials with active shortening.

For the trials with no active shortening, the amplitudes of the sinusoidal curve were 0.2%, 0.4%, 0.6%, 0.8%, 1%, and 3% of L_0 (Fig. 2.2B, blue), and for the trials with active shortening, the amplitudes were 1%, 3%, 5%, 7%, 9% and 11% of L_0 (Fig. 2.2A, blue). Activation was constant at ~35% of P_0 (Fig. 2.2A, B, red). Instantaneous muscle stiffness was measured using a quick length transient (0.9% L_0, 3 L_0/s) at L_0.

2.2.4 Data Analysis

Data were sampled at 4000 Hz and collected using a DAQ box (National Instruments, Austin, Texas, USA). Muscle stiffness, peak muscle force and peak muscle length during active shortening following submaximal isometric contraction were normalized to values measured at P_0. The relative values were used for statistical analysis. Differences were considered significant as the $p < 0.05$ level and Tukey's honestly significant difference (HSD) test was used to evaluate *post hoc* differences among means. All data are reported as means ± S.D.

In protocol 1, two-way ANOVA was used to test if active shortening and different

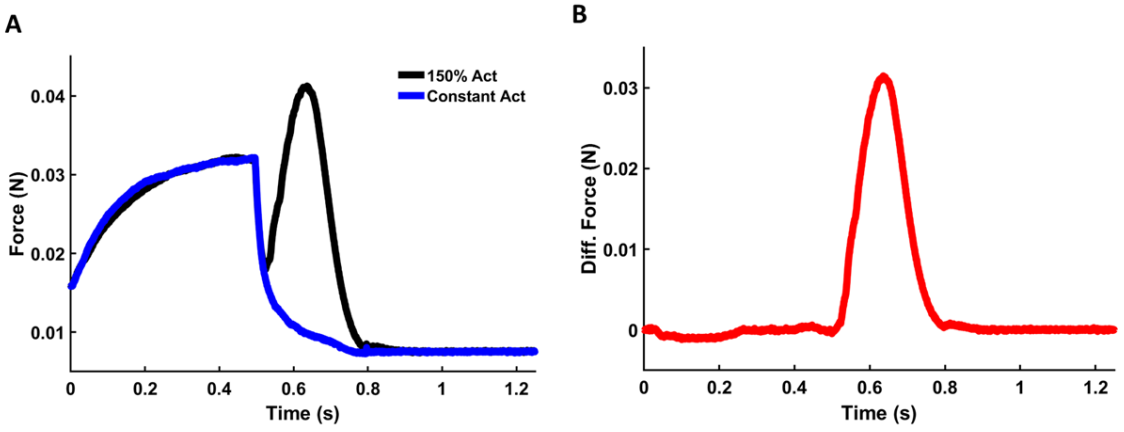

Figure 2.3: A) Raw force traces from protocol 1 at a shortening velocity of 0.5L_0/s for constant activation (blue) and time-varying activation (black). After muscles reached steady-state force, they shortened actively, which caused muscle force to decrease. At the onset of shortening, the amplitude of activation was increased. **B)** In order to evaluate the effect of activation on muscle force, muscle force with constant activation was subtracted from muscle force with time-varying activation (red).

activation amplitude induce changes in muscle stiffness. To evaluate the relationship between variable muscle stiffness and force resulting from active shortening at different activation amplitudes, the correlation coefficient between muscle stiffness and force was calculated using standard linear regression. Muscle force with time-varying activation was subtracted from muscle force with constant activation (Fig. 2.3). The peak force after subtraction (Fig. 2.3B) was used to analyze the effect of shortening velocity and activation on muscle force during active shortening. Analysis of covariance (ANCOVA) was performed to identify changes in mean peak force, with shortening velocity as the covariable and amplitude of activation as the main effect.

In protocol 2, one-way ANOVA was performed to investigate the effect of shortening velocity on muscle stiffness. ANCOVA was used to test the effects of length perturbation and shortening velocity on muscle force, with shortening velocity as the covariable and length perturbation as the main effect.

2.3 Results

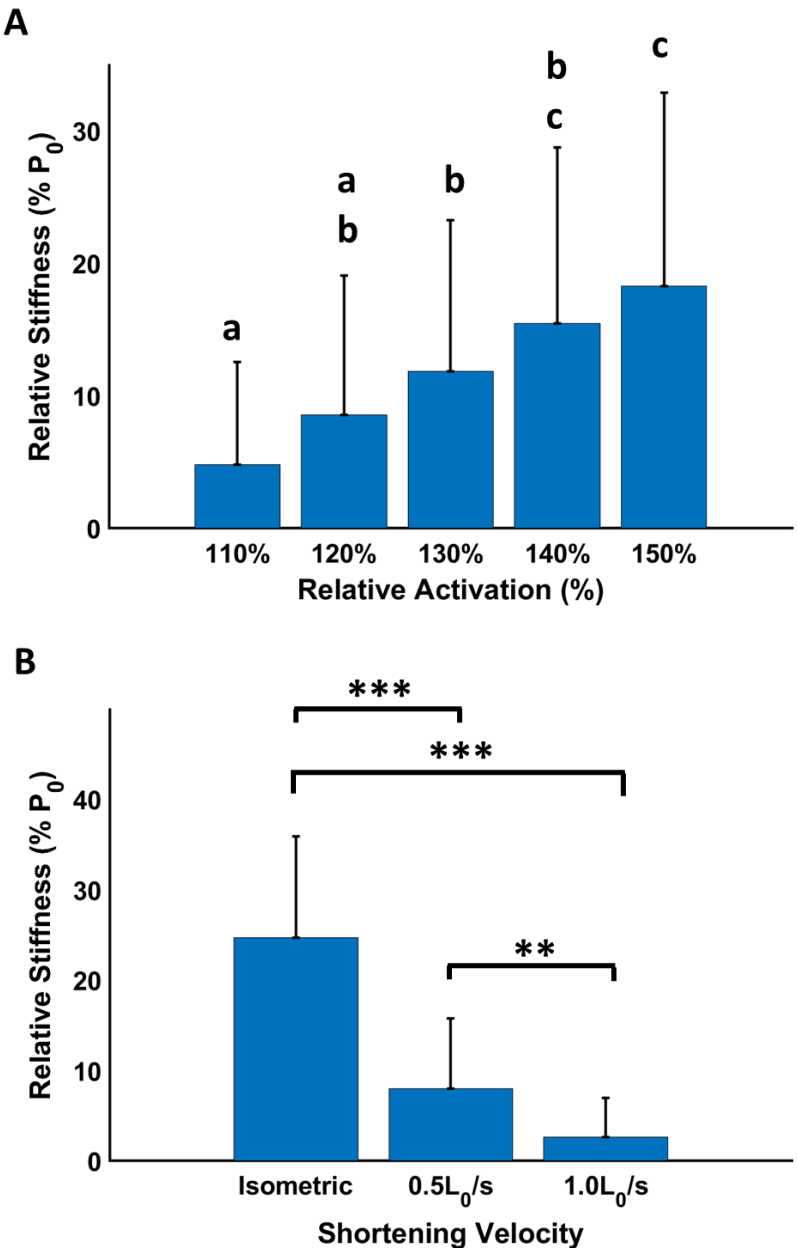

Figure 2.4: Mean values (+1 SD) of relative stiffness after (A) different activations and (B) different velocities of active shortening. Muscle stiffness was measured at L0 during active shortening following submaximal isometric contraction. Relative activation indicates peak amplitude of time-varying activation normalized to the activation amplitude measured for the submaximal isometric contraction. Mean relative stiffness increased with increasing amplitude of activation and decreasing shortening velocity. Bars not connected by the same letter are significantly different (HSD, $p < 0.05$). $^{*}p < 0.05$, $^{**}p < 0.01$ and $^{***}p < 0.001$.

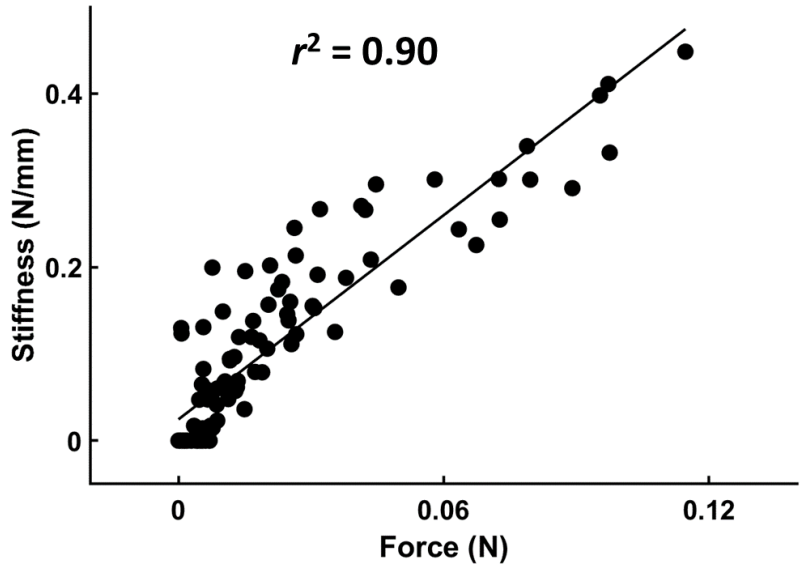

Figure 2.5: Muscle stiffness correlates with muscle force (r^2 = 0.90, p < 0.001). Muscle stiffness was measured at L_0 during active shortening at different velocities following submaximal isometric contraction. Time-varying activation at six different amplitudes was performed during active shortening.

We used two protocols to test the hypotheses that muscle stiffness varies with shortening velocity, and that muscle stiffness affects the force response to changes in activation amplitude (protocol 1) and length perturbations (protocol 2). In protocol 1, we used time-varying activation during active shortening to quantify the effect of activation amplitude on muscle force. In protocol 2, various amplitudes of length perturbation were applied to muscle during active shortening to investigate the effect of muscle stiffness on the force response of muscle to length perturbations.

2.3.1 Protocol 1

Relative muscle stiffness significantly increased with increasing activation amplitude ($F = 13.28$, $p < 0.001$) and decreasing shortening velocity ($F = 102.57$, $p < 0.001$). The interaction between activation amplitude and shortening velocity on muscle stiffness was not significant ($F = 1.18$, $p = 0.32$). Relative muscle stiffness at the highest activation amplitude

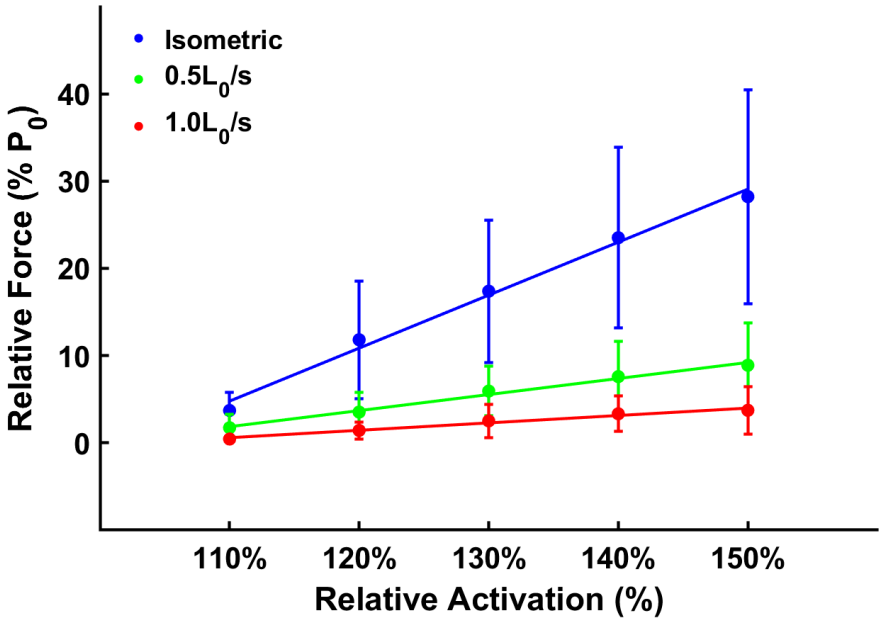

Figure 2.6: Amplitude of activation vs. relative force at different active shortening velocities. Data points (n = 7 muscles per group) are means across muscles with error bars representing SD. The slope of the relationship between amplitude of activation and relative force differed significantly among shortening velocities (ANCOVA, slope $p < 0.001$) but the y-intercept was not significantly different. Lines show regression of mean values.

(150% of activation amplitude at the first submaximal isometric contraction) was significantly higher than at 130% (HSD, $p < 0.05$), 120% (HSD, $p < 0.01$) and 110% (HDS, $p < 0.001$) (Fig. 2.4A). Stiffness at 140% was significantly higher than at 120% (HSD, $p < 0.05$) and 110% (HSD, $p < 0.001$), stiffness at 130% was significantly different from 110% (HSD, $p < 0.01$) (Fig. 2.4A). All shortening group means were significantly different from each other (HSD, $p < 0.001$) (Fig. 2.4B). Linear regression analysis showed a significant correlation between

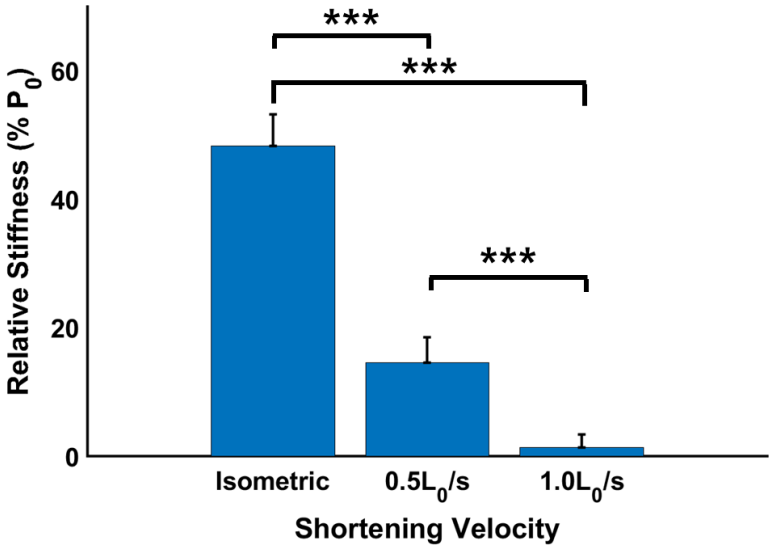

Figure 2.7: Mean values (+1 SD) of relative stiffness at L0 after different velocities of active shortening (n=6). Mean stiffness decreased significantly (HSD, $^{***}p < 0.001$) with increasing shortening velocity.

muscle stiffness and force ($r^2 = 0.82$, $p < 0.001$; Fig. 2.5).

In the relationship between the maximum force and activation amplitude, the slope differed significantly among shortening velocities (ANCOVA, $F = 16.96$, $p < 0.001$). The slope for isometric contractions was greater than the slope at 0.5 L_0/s (HSD, $p < 0.001$) and 1.0 L_0/s (HSD, $p < 0.001$) (Fig. 2.6) The intercept did not differ significantly among shortening velocities.

2.3.2 Protocol 2

ANOVA demonstrated a significant effect of shortening velocity on muscle stiffness ($F = 199.17$, $p < 0.001$). All shortening velocity group means were significantly different from each other (HSD, $p < 0.001$; Fig. 2.7). As in protocol 1, muscle stiffness significantly decreased with increasing shortening velocity.

For the relationship between length perturbation amplitude and maximum force, the

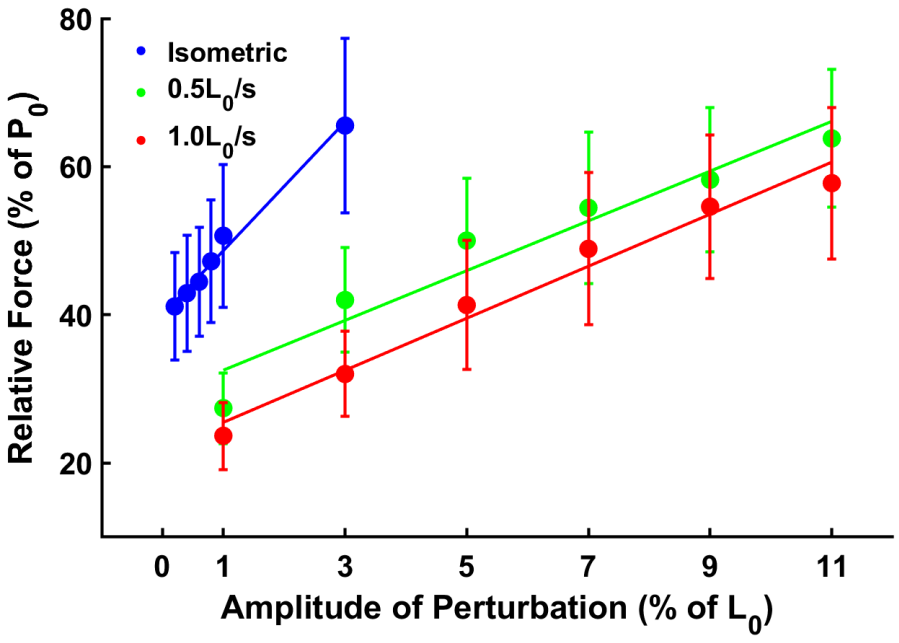

Figure 2.8: Amplitude of length perturbations vs. relative force at different active shortening velocities. Data points (n = 5 muscles per group) are means across muscles with error bars representing SD. The slope and intercept of the relationship between amplitude of length perturbation and relative force differed significantly among shortening velocities (ANCOVA, slope $p < 0.05$, y-intercept $p < 0.001$). Lines show regression of mean values.

intercept and the slope differed significantly among shortening velocities (ANCOVA, $F = 33.29$, $p < 0.001$, y-intercept; ANCOVA, $F = 4.13$, $p < 0.05$, slope). For the isometric condition, the maximum force increased faster with length perturbation amplitude than for $0.5L_0$/s (HSD, $p < 0.05$) and $1.0L_0$/s (HSD, $p < 0.05$) (Fig. 2.8). Additionally, the isometric condition had a greater y-intercept than $0.5L_0$/s (HSD, $p < 0.05$) and $1.0L_0$/s (HSD, $p < 0.001$) (Fig. 2.8). There was no significant difference of slope or y-intercept between $0.5L_0$/s and $1.0L_0$/s.

2.4 Discussion

It has been proposed that the contribution of activation to muscle force depends on muscle length (Daley and Biewener, 2011; Daley et al., 2009; Sponberg et al., 2011a; Sponberg et al., 2011b). In isometric conditions, activation is primarily responsible for the control of muscle force (Inman et al., 1952; Seyfert and Künkel, 1974; Smith and Stokes, 1993), whereas the contribution of activation to force is dependent on length history under dynamic conditions. Additionally, muscle responds differently to length perturbation depending on length history (Libby et al., 2020). The effect of length history should be to change muscle stiffness because different length history causes different muscle force and muscle force has a linear correlation with muscle stiffness (Kirsch et al., 1994). In the force velocity relationship, as active shortening velocity increases, force decreases. Greater shortening velocity will result in the lower muscle stiffness. Here, we tested the effect of active shortening on muscle stiffness, and then the force response of muscle to activation and length perturbations depending on muscle stiffness.

2.4.1 Protocol 1

In order to evaluate the contribution of activation to muscle force depending on muscle stiffness, we focused on two points: 1) how muscle stiffness is affected by shortening velocity, and 2) how varied muscle stiffness, resulting from active shortening at different velocities affects, the relationship between muscle force and activation.

Active shortenings at different velocities following submaximal isometric contraction were performed to vary muscle stiffness. Muscle stiffness significantly decreased with increasing shortening velocity (Fig. 2.4B) and decreasing activation amplitude (Fig. 2.4A). The reduced muscle stiffness can be explained by the decrease in muscle force ($r^2 = 0.90$, $p < 0.001$;

Fig. 2.5) in agreement with a previous study (Kirsch et al., 1994; Sugi and Tsuchiya, 1988). The results suggest that muscle stiffness is regulated by shortening velocity and activation. If muscles had different length and activation history, they would show different stiffness even at same length.

Based on the relationship between activation amplitude and muscle stiffness, we evaluated how active shortenings at different velocities affect the force response of muscle to activation. In our results, muscle was more sensitive to activation amplitude in isometric conditions than in active shortenings (Fig. 2.6). Muscle force increased significantly faster with increasing activation amplitude in isometric contractions (Fig. 2.6, blue) than in active shortenings (Fig. 2.6, green and red). Since muscle stiffness decreases as shortening velocity increases, the results can be interpreted that the relative contribution of activation to muscle force decreases with decreasing muscle stiffness.

2.4.2 Protocol 2

As in protocol 1, we investigated two points: 1) how active shortening changes muscle stiffness and 2) how the muscle stiffness affects the effect of length perturbations on muscle force. To evaluate those two points, length perturbations were performed following active shortening at different shortening velocities. Muscle stiffness was measured at the onset of length perturbations.

Muscle stiffness decreased with increasing shortening velocity (Fig. 2.7). The result was consistent with the results of protocol 1. The effect of length perturbations on muscle force was dependent on shortening velocity (Fig. 2.8). When shortening velocity increased, the greater length perturbation was needed to produce the same force. Furthermore, muscle force increased faster with increasing the amplitude of length perturbations in isometric contraction

(Fig. 2.8, blue) than in active shortenings (Fig. 2.8, green and red). When linked these results with the relationship between shortening velocity and muscle stiffness, the effect of length perturbations on muscle force is affected by muscle stiffness at the onset of the perturbation. The greater muscle stiffness produces the greater peak force during length perturbations in same length and activation.

2.4.3 Changes in force potential in the force-velocity relationship

The reduced force potential caused by active shortening would induce the effects of activation on force to decrease. According to the force-velocity relationship of soleus muscle of rat, the maximal forces at $0.5L_0$/s and $1.0L_0$/s were about $0.3P_0$ and $0.2P_0$, respectively (Claflin and Faulkner, 1989). Chow and Darling, (1999) showed the variable force-velocity relationship at different activation levels. When decreasing in shortening velocity, muscle force increased more with increasing activation level. Although the contraction type in their study was not isotonic but isovelocity, the shape of the force-velocity relationship developed by isovelocity data was similar to the relationship by isotonic data (James and Johnston, 1998). Thus, the reduced contribution of activation to muscle force is partially due to the decreased force potential.

2.4.4 A composite material viewpoint as one alternative muscle viewpoint

In the traditional viewpoint of muscle as a motor, muscle force is mainly controlled by activation, length, and velocity of muscle (Hof and Van den Berg, 1981; Olney and Winter, 1985; van Ruijven and Weijs, 1990). For example, the ‘Hill-type’ muscle model determines muscle force by activation level, isometric force-length and isotonic force-velocity

relationships (Dick et al., 2017; Wakeling et al., 2021). In this viewpoint, the muscle forces fail to predict the history dependence of muscle force (Perreault et al., 2003; Sandercock and Heckman, 1997) because they should produce same force at the same length and activation. It seems hard to reconcile our findings with this model in that muscle can produce different force depending on its stiffness even with same length and activation. The traditional viewpoint would not explain our findings unless it takes account of the history dependent stiffness.

A composite material viewpoint could be one of alternative muscle viewpoint because it is able to reflect tunable elasticity of muscle depending on length history. Libby et al. (2020) presents that the force response of muscle to length perturbation is history dependent, suggesting muscle has a different viscoelastic memory by length history. They developed a simple material model including a spring and a damper to predict the force response of muscle. When the equilibrium length of the spring is proportional to preload, the model predicts the work quantity during length perturbation very accurately ($r^2 > 0.99$).

The variable equilibrium length of the spring can be replaced with tunable stiffness, as both affect the spring force. We developed the similar three-parameter viscoelastic model including a linear spring and a linear damper which are in parallel, but the spring stiffness was proportional to the measured muscle stiffness, instead of the equilibrium length proportional to preload (Fig. 2.9). Because the measured muscle stiffness depended on shortening velocity (Fig. 2.7), the tunable stiffness can be referred as the history dependent stiffness. The parameter sets were optimized for the best r^2 value for length perturbations using all subject data in protocol 2 and then the models predicted each subject data in protocol 2 using the optimized parameter sets. Work magnitude during length perturbation was predicted accurately (mean $r^2 = 0.92 \pm 0.08$) by the model with tunable stiffness as in the previous study (Libby et al., 2020), and the

model with constant spring stiffness also predicted muscle work output accurately (mean r^2 = 0.90 ± 0.09) (Fig. 2.9. A & B). Since this study has focused on peak muscle force, the peak force was also predicted by the model with the same parameter set. The model including tunable stiffness did fit better with the peak force (mean r^2 = 0.77 ± 0.05) than the model including constant stiffness (mean r^2 = 0.42 ± 0.26) (Fig. 2.9. C & D). The viscoelastic model with tunable stiffness captures the peak force as the response of length perturbation as well as work quantity. The simulated results support the suggestion that variable muscle force under dynamic conditions can be somewhat accurately predicted by the force response of a history dependent viscoelastic material to length perturbations. Therefore, to enlarge our understanding of how muscle adjusts to dynamic conditions, we need the alternative muscle viewpoint which can reflect the tunable stiffness. A composite material muscle viewpoint should be considered as one alternative muscle viewpoint.

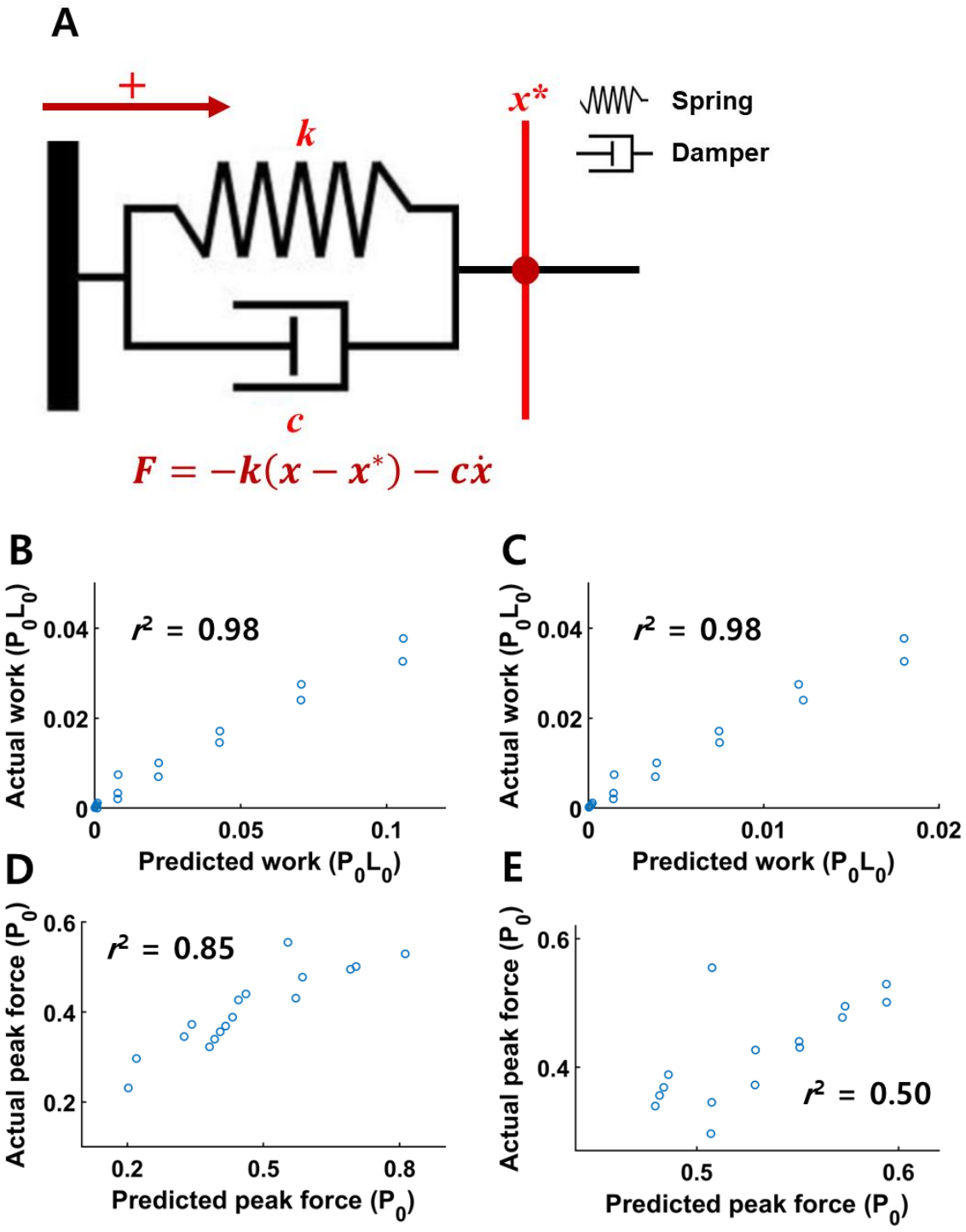

Figure 2.9: Schematic of three-parameter viscoelastic model (A), one example of predicted work (B & C), and one example of predicted peak force (D & E). (A) The viscoelastic model predicts muscle force during length perturbations depending on a spring constant, *k*, a damping coefficient, *c*, and the equilibrium position, *x**. *k* is proportional to its own measured stiffness (B & D), while *c* and *x** are constant. For a comparison, the model with no tunable spring constant predicts work and peak muscle force during length perturbations (C & E).

2.4.5 Application to locomotion

While muscle adopts a variety of roles during locomotion in steady state depending on the phase of activation or loading (Ahn et al., 2006; Daley and Biewener, 2003; Dickinson et al., 2000; Roberts et al., 1997), uncertainty remains regarding how muscle adjusts to unsteady conditions which are common in natural settings. This study directly investigated the effects of length perturbations on muscle force depending on muscle stiffness.

In vivo data from Daley and Biewener (2011) offer an unique opportunity to evaluate how muscle force is controlled in uneven terrains. They measured *in vivo* force, strain, and activation of guinea fowl lateral gastrocnemius (LG) during treadmill running over obstacles. Peak LG force in stance phase was varied to overcome obstacles. When stepping up the obstacles, the peak LG force usually was greater, but when stepping down, the force was less than during level walking. Interestingly, the peak force is more closely correlated with length at foot contacts ($r^2 = 0.63$; Fig. 2.10), than peak electromyography (EMG) intensity ($r^2 = 0.34$; Fig. 2.10). Because EMG and length trajectory before foot contact had relatively little stride-to-stride variation in respect to time due to the constant treadmill running speed (Fig. 2.11), length at foot contact would indicate the time phase of foot contact.

The effect of earlier foot contact for stepping up is to convert active shortening to isometric contraction earlier or to at least slow down shortening velocity earlier than other steps. Although foot contacts for obstacle strides happen earlier (Fig. 10, red circle) than for level running (Fig. 2.11, line (a)), we made the assumption that all strides have identical time phase of length perturbation (Fig. 2.11, line (a) & (b)) to interpret the varied peak force. The earlier conversion to isometric contraction allows for the bigger preload at the onset of length

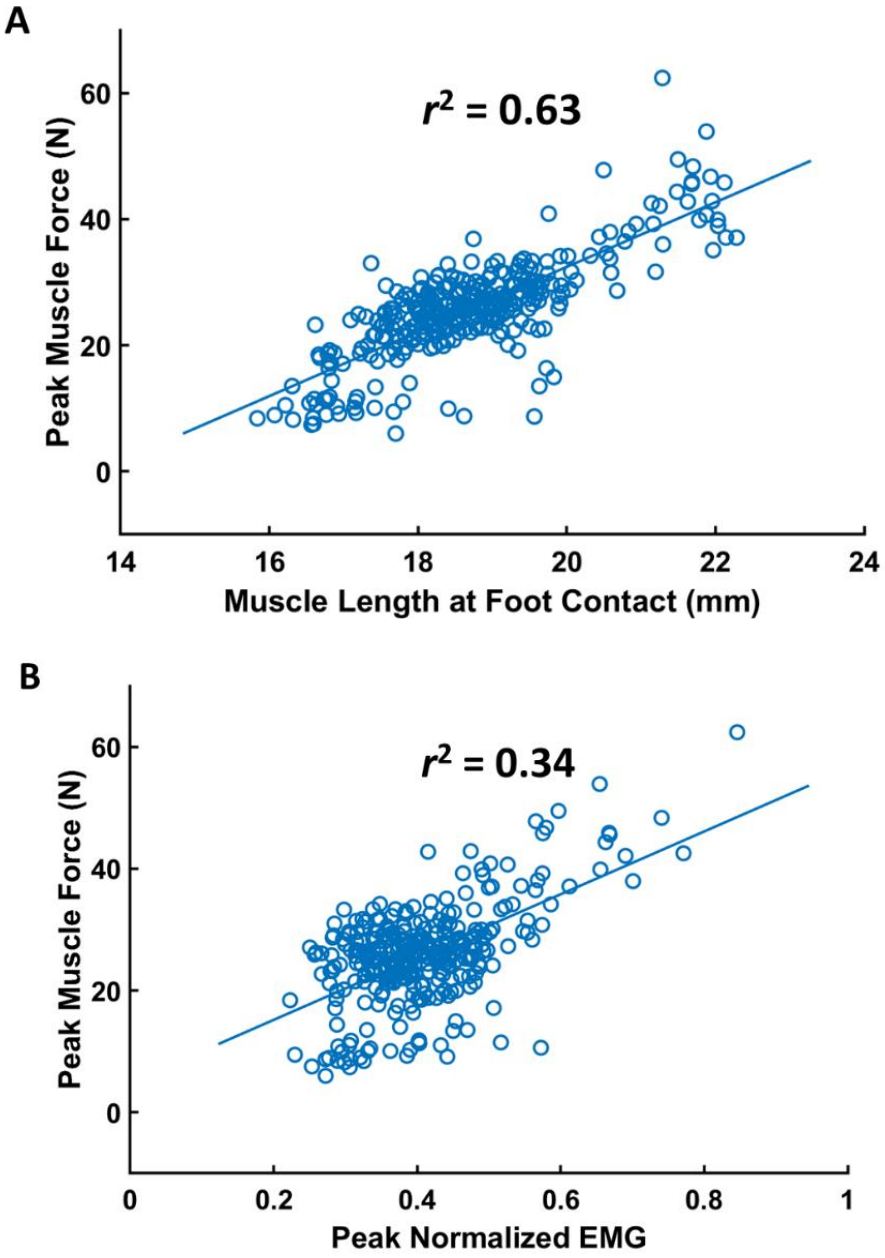

Figure 2.10: A) The relationship between peak muscle force and muscle length at foot contact for *in vivo* guinea fowl LG. Peak muscle force and muscle length at foot contact were extracted from all steps from a single bird (n = 320). Peak muscle force was linearly related to muscle length at foot contact (r^2 = 0.63). **B) The relationship between peak muscle force and peak normalized EMG.** Peak normalized EMG value was extracted from all steps. The r^2 value between peak normalized EMG and peak muscle force was 0.34. Data from Daley and Biewener (2011).

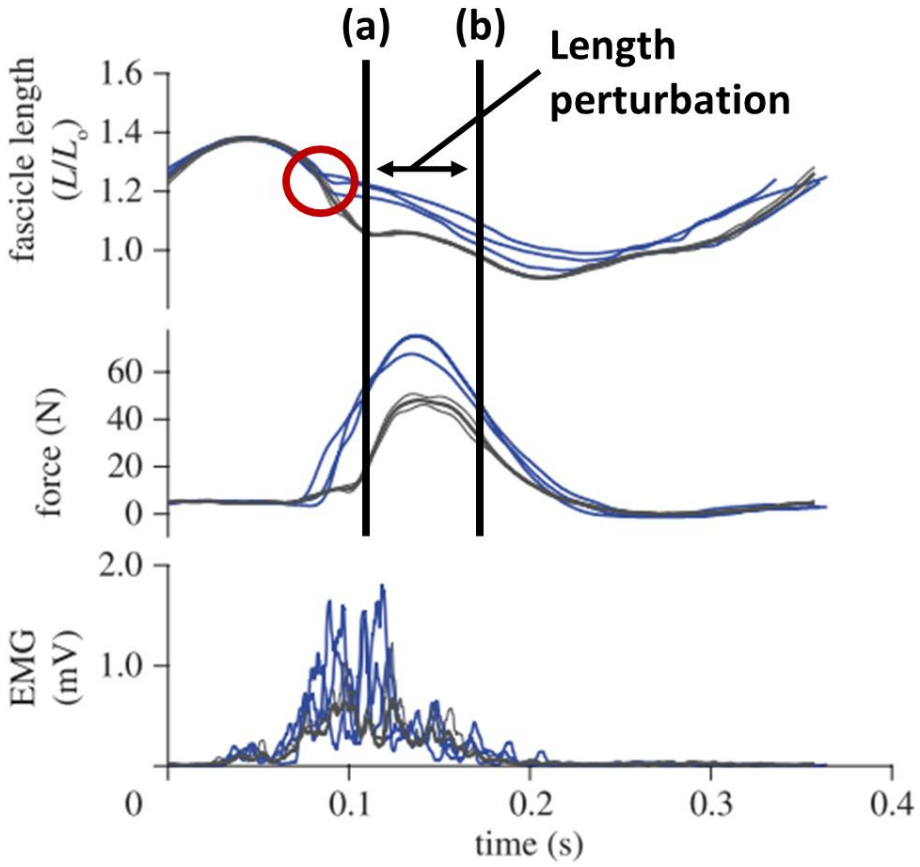

Figure 2.11: Changes in *in vivo* LG length, force, and EMG (mean ± SE) vs. time during treadmill running in guinea fowl. Level running (gray lines) vs. running over 5cm obstacles (blue lines). Red circle and Line (a) indicate foot contacts for running over obstacles and for level running, respectively. Distance between line (a) and (b) represents the length perturbation period. Foot contacts for running over 5cm obstacles (blue lines) occur earlier than for level running (gray lines). Obstacle steps show greater force at the onset of length perturbation than level steps. Graph reproduced from Daley and Biewener (2011).

perturbations (Fig 2.11, line (a)), which results in the greater peak force. Preload refers to force at the onset of length perturbation. The interpretation is in accordance with the previous study that work during length perturbation depends on preload (Libby et al., 2020). If the preload can be replaced with its muscle stiffness, the varied peak LG force can reconcile our findings in this study that greater muscle stiffness has more sensitive to length perturbation. In addition, the low r^2 value between peak muscle force and peak EMG intensity (Fig. 2.10B) is also

supported with our results in that the effect of activation on muscle force is relatively little during active shortening. In sum up, our results and the guinea fowl data have demonstrated that the varied peak force during active shortening is determined by the variable force response to length perturbation depending on history dependent muscle stiffness, and the varied peak force cannot be explained solely by activation.

2.4.6 Conclusion

In this study, we found that muscle has tunable stiffness determined by length history, and the tunable stiffness causes muscle to differently respond to activation or length perturbations between isometric and dynamic conditions. These findings suggest that a new alternative muscle viewpoint is required to reflect the tunable stiffness. A composite material viewpoint could be the alternative viewpoint in that it is able to implement the tunable stiffness. The simple material model including the history dependent muscle stiffness can accurately predict our data. Also, our findings can be used to analyze the varied peak force of plantar flexors during locomotion on uneven terrain. The varied peak force is related with length at foot contact. The length at foot contact indicates force at the onset of length perturbation. If force implies muscle stiffness, the force response of muscle to deformation by external force is dependent on its stiffness. Our findings support the interpretation of the varied peak force.

Chapter 3. The effect of active shortening at different velocities on ratio of muscle stiffness to force during force redevelopment

3.1 Background

The muscle stiffness (k_m) to muscle force (F_{ISO}) ratio (SFR) is believed to be relatively constant during isometric contraction at a given muscle length and neural activation level, because both isometric muscle force and muscle stiffness are considered to be linearly related to the number of attached cross bridges (Ford et al., 1981; Gordon et al., 1966; Huxley and Niedergerke, 1954). However, Julian and Morgan (1981) found that the SFR was altered during isometric force redevelopment after active shortening. During isometric contraction following active shortening, k_m was greater than in a purely isometric contraction at the same length (Julian and Morgan, 1981). If k_m is primarily related to cross-bridge stiffness and stiffness of passive structures, then active shortening before isometric contraction may affect either cross-bridge stiffness or passive stiffness, or both.

Assuming the same number of attached cross bridges for isometric contraction at the same muscle length and force, the greater k_m in the isometric redevelopment period cannot be explained solely by cross bridges. However, weakly-bound cross bridges make it possible to explain the greater k_m at the same muscle force without additional changes in the stiffness of passive structures. It has been hypothesized that weakly-bound cross bridges are generated in the newly forming overlap zone between actin and myosin during active shortening (Maréchal and Plaghki, 1979). Although the weakly-bound cross bridges do not produce force, they contribute to k_m (Huxley, 1957; Joumaa et al., 2012). This property of weakly-bound cross

bridges would increase k_m at a given F_{ISO}, increasing the SFR.

The greater k_m following active shortening could also be associated with changes in titin stiffness. Rassier and Herzog (2004) suggested that the equilibrium length (zero force) of a parallel element is adjusted when force redevelops isometrically following active shortening. They showed not only that the amount of force enhancement is affected by active shortening prior to active lengthening, but also that the effect of shortening on force enhancement is reduced by increasing the duration of a pause between shortening and lengthening. The parallel element is likely to be titin because titin is in parallel with attached cross bridges (Herzog, 2018). If titin is assumed to be a linear spring whose force is related to the amount of force enhancement (Herzog, 2018; Nishikawa, 2020), then increasing force enhancement with pause duration could be associated with increased titin force caused by the adjustment of titin equilibrium length.

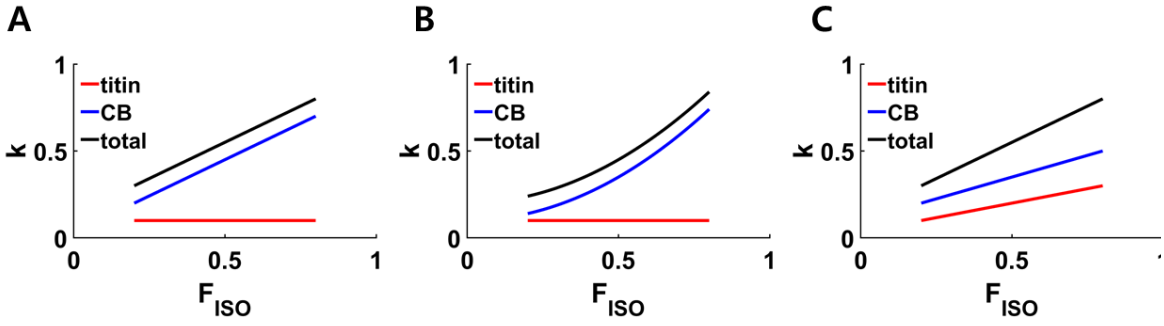

Figure 3.1: **Theoretical relationships between relative muscle stiffness (k_m) and relative muscle isometric force (F_{ISO}).** Total muscle stiffness (black) is calculated as the sum of titin stiffness (red) and cross-bridge (CB) stiffness (blue). A) If the proportion of weakly-bound to strongly-bound cross bridges is independent of F_{ISO} and titin stiffness is constant, then the relationship between km and F_{ISO} will be linear. B) If titin stiffness is constant but the proportion of weakly-bound to strongly-bound cross bridges depend non-linearly on F_{ISO}, then the total stiffness will also increase non-linearly with F_{ISO}. (C) Both titin stiffness and the proportion of weakly-bound to strongly-bound cross bridges increase linearly with F_{ISO}, so the total stiffness also increases linearly with F_{ISO}.

Theoretically, weakly-bound cross bridges and/or a change in titin stiffness or equilibrium length can explain the increase in SFR after active shortening. However, supporting experimental evidence for either hypothesis is absent. Information on the number of weakly-bound cross bridges and/or titin behavior in the active state could potentially be inferred from the change in SFR during isometric contraction after shortening. In the relationship between k_m and $F_{ISO,}$ the y-intercept might be related to either the quantity of weakly-bound cross bridges, or titin stiffness, or both, since the y-intercept is the stiffness at zero force. In addition, the slope represents how the proportion of weakly-bound cross bridges to strongly-bound cross bridges and/or titin stiffness change when isometric force redevelops during the pause following active shortening (Fig. 1). If the proportion of weakly to strongly-bound cross bridges is constant throughout the redevelopment period with constant titin stiffness, or alternatively if titin stiffness depends linearly on F_{ISO}, then the slope should be linear. Otherwise, the slope should be non-linear due to the changing proportion of strongly-bound cross bridges and/or non-linear dependence of titin stiffness on F_{ISO}.

Shortening at different velocities changes the SFR because F_{ISO} decreases more rapidly with shortening velocity than k_m (Julian and Sollins, 1975). Therefore, according to Julian and Sollins (1975), the y-intercept of the relationship between k_m and F_{ISO} should increase with decreasing shortening velocity. However, the shape of the slope is not predicted easily since there is no generally accepted mechanism that explains the change in SFR during isometric contraction after active shortening. The aim of this study was to systematically investigate how SFR changes during the isometric force redevelopment period following active shortening at different shortening velocities. Results may provide insights about how the proportion of weakly-bound to strongly-bound cross bridge and/or titin stiffness change during force

redevelopment after active shortening. We designed an experiment in which muscles first develop force isometrically, and are then shortened at different velocities, followed by a period of isometric force redevelopment during which F_{ISO} and k_m were measured.

3.2 Materials and Methods

3.2.1 Animals

Mice of the strain B6C3Fe a/a-Ttn^{mdm}/J were obtained from the Jackson Laboratory (Bar Harbor, ME, USA) and a breeding colony was established in the animal care facility at Northern Arizona University (NAU). Soleus muscles from homozygous wild-type mice (n=7; female = 2, male = 5; mass = 23.31±1.38g) were used in this study. The Institutional Animal Care and Use Committee at NAU approved the experimental protocol and use of animals.

3.2.2 Muscle preparation

Wild-type mice were euthanized by isoflurane overdose, confirmed by cervical dislocation. Soleus muscles were isolated and the tendons at the muscle-tendon junction were tied with 4-0 silk suture as close as possible to the muscles to reduce contributions of extramuscular connective tissue. The muscles were attached to an inflexible hook at one end and to a servomotor length and force controller (Aurora Scientific, Inc., Series 300B, Aurora, ON Canada) at the other. Muscles were placed in an experimental chamber filled with mammalian Krebs-Ringer solution (in mM: 137 NaCl, 5 KCl, 1 NaH_2PO_4, 24 $NaHCO_3$, 2 $CaCl_2$, 1 $MgSO_4$, and 11 dextrose, pH 7.4; buffered with 95% O_2 and 5% CO_2) at 22 °C.

Stimulation was achieved using two platinum electrodes placed parallel to the muscle in the chamber. For maximal tetanic stimulation, square wave pulses at 60 V were delivered to the muscles at a frequency of 75 Hz using a Grass S48 stimulator. To determine optimal muscle length (L_0), muscles were activated using maximal tetanic stimulation and muscle length was adjusted until maximum isometric muscle force (P_0) was established. Maximum isometric force, measured at the end of the experiments, was within 15% of the maximum isometric force

measured at the beginning of the experiments for all muscles.

3.2.3 Experimental protocols

Maximal isometric force at 1.05 L_0 was established for whole soleus muscles isolated from wild-type mice (Fig. 3.2, bottom). The muscles were actively shortened to L_0 at three velocities (1/8 L_0/s, ½ L_0/s and 2 L_0/s) and then held isometrically for four pause durations (10, 20, 80 and 1000 ms) which allowed isometric force redevelopment (Fig. 3.2, top). To measure instantaneous muscle stiffness, quick transients (0.9% L_0 stretch at a speed of 3 L_0/s) were conducted at the end of the pause. For a comparison, the muscle stiffness was also measured during isometric contractions at L_0 without active shortening at similar durations after the onset of stimulation (10, 20, 80 and 1000 ms). The order of the different velocities and pause

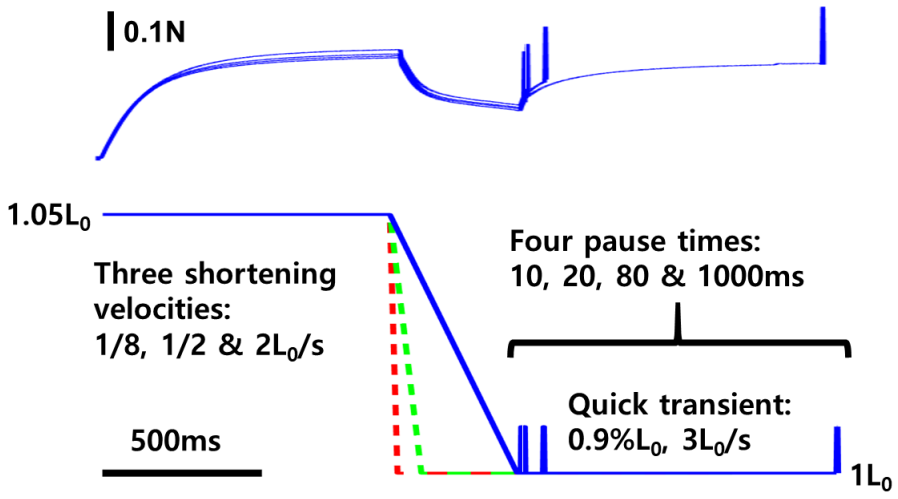

Figure 3.2: Muscle force (upper trace), length (lower trace) and measurement of instantaneous muscle stiffness. Protocols used to evaluate the effects of active shortening and duration of isometric redevelopment on muscle stiffness and force. Active shortening was performed from 1.05L_0 to L_0 at three different velocities; 1/8 L_0/s (red), ½ L_0/s (green) and 2 L_0/s (blue). Instantaneous muscle stiffness was measured using quick stretch with an amplitude of 0.9% L_0 and a velocity of 3L_0/s at four different pause durations (10, 20, 80 and 1000 ms).

durations was randomized for each muscle. A period of 4.5 min rest was given between trials. Instantaneous muscle stiffness was calculated as the change in muscle force during the quick stretch, divided by the amplitude of the quick stretch (Fig. 3.2).

3.2.4 Data Analysis

Data were sampled at 4000 Hz and collected using a DAQ box (National Instruments, Austin, Texas, USA). Muscle stiffness (k_m) and isometric force (F_{ISO}) at the end of the pause were normalized by the values measured at 1000 ms without active shortening, and the relative values were used for statistical analysis. All data are shown as means ± S.E. Two-way ANOVA was used to determine differences in F_{ISO} and k_m among different shortening velocities and pause durations. The main effects were shortening velocity and pause duration. The effects of shortening velocity and F_{ISO} on k_m were tested using analysis of covariance (ANCOVA), with F_{ISO} as the main effect and active shortening velocity as the covariable. Tukey's honestly significant difference (HSD) test was used to evaluate *post hoc* differences among means.

3.3 Results

Both relative muscle force (F_{ISO}) and muscle stiffness (k_m) increased during the period of isometric force redevelopment following active shortening (Fig. 3.3A and C). The rate of increase in both F_{ISO} and k_m during the force redevelopment period depended on shortening velocity (Fig. 3.4). The muscle stiffness to force ratio (SFR) also differed depending on shortening velocity, showing different y-intercepts and slopes for different shortening

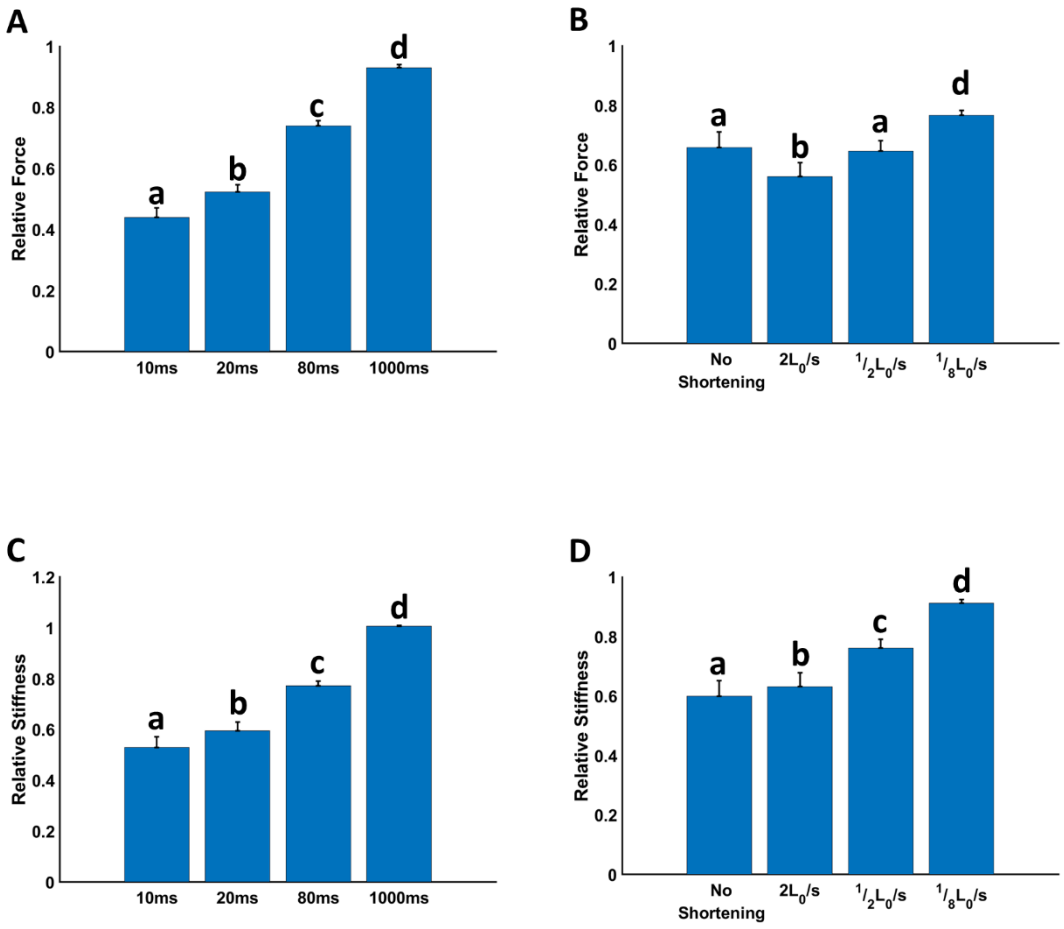

Figure 3.3: Mean values (+ 1 S.E.) of relative force (A, B) and relative stiffness (C, D) after different pause durations (A, C) and different velocities of active shortening (B, D). Both mean relative force and stiffness increased with increasing pause duration and decreasing shortening velocity. Bars not connected by the same letter are significantly different (HSD, $p < 0.001$).

Table 3.1: Results of two-way ANOVA. Effects of pause duration (10, 20, 80 and 1000 ms) and shortening velocity (1/8, ½, and 2 L_0/s) on relative muscle force.

	Df	Sum Sq	Mean Sq	F-Value	P-Value
Pause duration	3	4.09	1.36	712.78	< 0.001
Shortening velocity	3	0.60	0.20	104.26	< 0.001
Interaction	9	0.71	0.08	41.03	< 0.001
Error	96	0.18	0.0019		
Total	111	5.58			

velocities in the $F_{ISO} - k_m$ relationship (Fig. 3.5).

ANOVA demonstrated significant effects of shortening velocity ($p < 0.001$), pause duration ($p < 0.001$), and their interaction ($p < 0.001$) on F_{ISO} (Table 3.1). All pause duration group means and shortening velocity group means were significantly different from each other

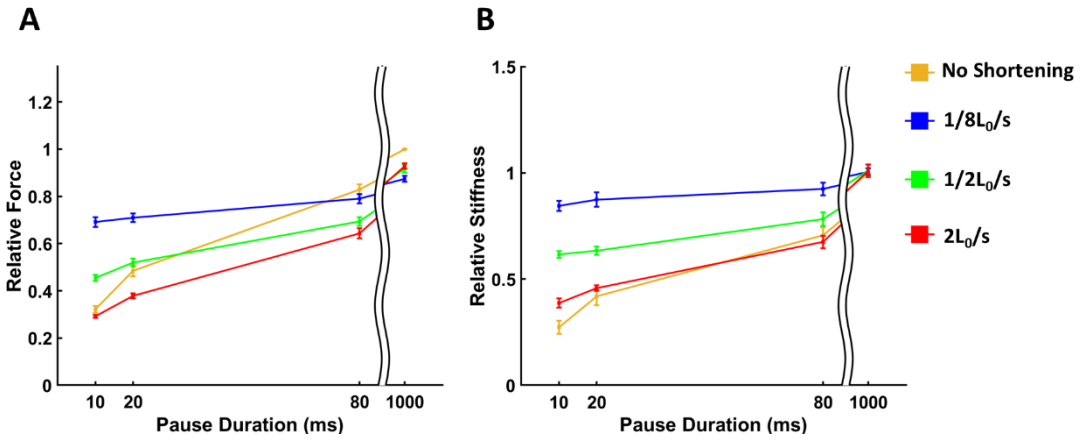

Figure 3.4: Change in relative muscle force and stiffness during isometric force redevelopment following active shortening at different velocities. Data points (n = 7 muscles per group) are means across muscles with error bars representing S.E. (A) Relative force increases with increasing pause duration. The rate of increase varies with shortening velocity. (B) Relative stiffness increases with increasing pause duration, and shortening velocity affects the stiffness vs. pause duration relationship. The slope of the relationship increases with increasing shortening velocity.

Table 3.2: Results of two-way ANOVA. Effects of pause duration (10, 20, 80 and 1000 ms) and shortening velocity (1/8, ½, and 2 L_0/s) on relative stiffness.

	Df	Sum Sq	Mean Sq	F-Value	P-Value
Pause duration	3	3.81	1.27	1767	< 0.001
Shortening velocity	3	1.70	0.57	787.79	< 0.001
Interaction	9	0.82	0.09	126.66	< 0.001
Error	96	0.07	0.00072		
Total	111	6.39			

except for 'no shortening' and '1/2 L_0/s' (Fig. 3.3A and B, HSD, $p < 0.001$). F_{ISO} increased with increasing pause duration and decreasing shortening velocity.

For the F_{ISO}-pause duration relationship, the slope of 'no shortening' was the steepest and the slopes of the active shortening group varied with shortening velocity (Fig. 3.4A). The

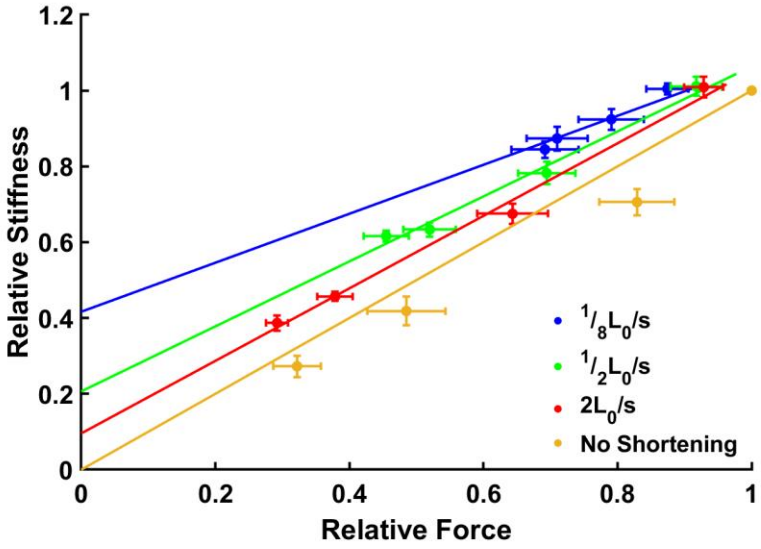

Figure 3.5: Relative force vs. relative stiffness at different active shortening velocities. Data points (n = 7 muscles per group) are means across muscles with error bars representing S.E. The slope and the y-intercept of the relative stiffness-force relationship differed significantly among different shortening velocities, including 'no shortening' (ANCOVA, slope, $p < 0.001$; y-intercept, $p < 0.001$).

Table 3.3: Slope, intercept, and correlation coefficients (means ± S.D) for the linear relationship between muscle force and stiffness after shortening at three velocities (1/8, 1/2 and 2 L_0/s) and with no shortening.

Shortening Velocity	Slope	Intercept	Correlation
No shortening	1.00 ± 0.026	0.00 ± 0.019	0.98***
1/8 L_0/s	0.65 ± 0.054[a,b]	0.42 ± 0.041[c]	0.84***
1/2 L_0/s	0.86 ± 0.031	0.21 ± 0.022[c,d]	0.98***
2 L_0/s	0.96 ± 0.026	0.10 ± 0.019[c,e,f]	0.99***

[a] significantly smaller than 'No shortening' ($p < 0.01$).

[b] significantly smaller than '1/2 L_0/s' ($p < 0.01$).

[c] significantly bigger than 'No shortening' ($p < 0.001$).

[d] significantly smaller than '1/8 L0/s' ($p < 0.05$).

[e] significantly smaller than '1/8 L0/s' ($p < 0.001$).

[f] significantly smaller than '1/2 L0/s' ($p < 0.01$).

*** $p < 0.001$

effects of shortening velocity ($p < 0.001$), pause duration ($p < 0.001$), and interaction ($p < 0.001$) on k_m were also significant (Table 3.2). All pause duration and shortening velocity group means were significantly different from each other (Fig. 3.3C and D, HSD, $p < 0.001$). The rate of increase in stiffness during the force redevelopment period depended on shortening velocity. As for F_{ISO}, the slope of 'no shortening' was the steepest and the slopes of the active shortening group increased with increasing shortening velocity (Fig. 3.4B).

The slopes and y-intercepts of the relationship between F_{ISO} and k_m differed significantly among shortening velocities (Fig. 3.5, ANCOVA, F = 116.16, $p < 0.001$, y-intercept; ANCOVA, F = 10.67, $p < 0.001$, slope). At the slowest shortening velocity (1/8 L_0/s; Fig 3.5, blue), k_m increased more slowly with F_{ISO} than for the faster velocities (1/2 L_0/s, Fig. 3.5, green, $p < 0.05$; 2 L_0/s, Fig. 4, red, $p < 0.001$) and also more slowly than for the 'No

shortening' condition (Fig. 3.5, yellow, $p < 0.001$). All y-intercepts were significantly different from each other (Table 3.3). A significant positive correlation between F_{ISO} and k_m was observed for all active shortening velocities as well as 'No shortening' (Table 3.3, $p < 0.001$).

3.4 Discussion

The aim of this study was to investigate how the ratio of muscle stiffness (k_m) to force (F_{ISO}) changes during the period of isometric force redevelopment following active shortening at different velocities. Our main findings were that: 1) F_{ISO} and k_m increased during the force redevelopment period following active shortening (Tables 1 and 2, Fig. 3); 2) the rate of increase in F_{ISO} and k_m was affected by active shortening velocity (Fig. 4); and 3) the slope and the y-intercept of the relationship between F_{ISO} and k_m differed among different shortening velocities (Table 3 and Fig. 5).

The y-intercept of the relationship between F_{ISO} and k_m increased significantly with decreasing active shortening velocity, and the y-intercept for 'no shortening' was significantly lower than for the experiments with active shortening (Table 3 and Fig. 5). This finding supports previous reports which showed decreasing k_m with increasing shortening velocity (Julian and Sollins, 1975). The velocity-dependent y-intercept suggests that k_m is substantial when F_{ISO} is zero, and the stiffness to force ratio is not constant for isometric contractions following active shortening.

According to the cross-bridge theory, k_m should be zero at zero force because F_{ISO} is a function of the number of attached cross bridges (Gordon et al., 1966; Huxley and Niedergerke, 1954). As expected, k_m equals 0 when F_{ISO} equals zero for the 'no shortening' protocol (Fig. 5, yellow). However, the 'active shortening' protocols showed non-zero y-intercepts that differed among the three shortening velocities (Fig. 5, blue, green, and red). These results are not consistent with the cross-bridge theory (Ford et al., 1981; Huxley, 1957). In order to explain the non-zero y-intercepts caused by active shortening, weakly-bound cross bridges have been invoked (Maréchal and Plaghki, 1979). The hypothesized mechanism postulates that weakly-

bound cross bridges form in the new overlap zone created by active shortening (Maréchal and Plaghki, 1979). As the weakly-bound cross bridges only contribute to k_m without producing force (Huxley and Simmons, 1971; Joumaa et al., 2012), the non-zero y-intercepts in the present study could potentially be explained by the weakly-bound cross bridges.

Previous studies found that force depression during shortening decreases with increasing shortening velocity (Herzog and Leonard, 1997; Leonard and Herzog, 2005; Maréchal and Plaghki, 1979), and proposed that the reduction of force is associated with the amount of stress imposed on actin filaments during active shortening (Joumaa et al., 2012). According to this hypothesis, the reduced stress on actin filaments caused by faster shortening results in binding of a smaller number of weakly-bound cross bridges to actin, which results in diminished force depression. The number of weakly-bound cross bridges increases with increasing actin stress produced by decreasing shortening velocity. Similar to these previous studies, the present study also found that that the slowest velocity resulted in the largest y-intercept between k_m and F_{ISO}, and also found that force depression decreases with increasing shortening velocity. These observations are potentially consistent with the hypothesis that more weakly-bound cross bridges are bound to actin when the shortening velocity is relatively slow.

In terms of the relationship between F_{ISO} and k_m, the three shortening velocities had different slopes (Fig. 5). If the velocity dependent y-intercept indicates the number of weakly-bound cross bridges, then the different slopes would suggest a different proportion of weakly-bound to strongly-bound cross bridges in the newly formed overlap zone. If the lower active shortening velocity results in greater stress and distortion of actin (Joumaa et al., 2012; Maréchal and Plaghki, 1979), this would increase the proportion of weakly-bound cross bridges. This mechanism can explain the observation that slower active shortening increased the y-

intercept of the stiffness-to-force relationship. However, it is not consistent with the reduced slope at the slower active shortening velocity. The greater distortion of actin developed by the slower active shortening velocity should increase the proportion of weakly-bound to strongly-bound cross bridges. The greater proportion should increase the slope because weakly-bound cross bridges only contribute to k_m without producing force. Therefore, the 'weakly-bound cross bridges' mechanism can explain the velocity-dependent y-intercept, but not the reduced slope at the slower active shortening velocity.

Another problem with the weakly-bound cross-bridge hypothesis is that it predicts a non-linear relationship between k_m and F_{ISO}. To produce a linear relationship between k_m and F_{ISO} during the force redevelopment period, the proportion of weakly- to strongly-bound cross bridges must be constant, and therefore the amount of actin distortion must also be constant during force redevelopment. Actin distortion has not been directly quantified after active shortening. Yet, previous studies have suggested that the amount of actin distortion depends on the amount of stress or work performed during shortening (Lee and Herzog, 2009; Maréchal and Plaghki, 1979). After shortening, since the stress is not constant and work is zero during the period of force redevelopment, the amount of actin distortion developed by active shortening should not be constant. The distorted actin should return toward its original state to some extent during the period of force redevelopment, and the proportion of weakly- to strongly-bound cross bridges should decrease. However, the slope was constant throughout the force redevelopment period except at the slowest velocity (Table 3), which suggests that actin distortion does not affect the proportion of weakly- to strongly- bound cross bridges. Therefore, the linear $F_{ISO} - k_m$ relationship cannot be explained solely by weakly-bound cross bridges.

Rassier and Herzog (2004) showed that active shortening prior to active lengthening

decreases the amount of force enhancement, and also that increasing the pause duration between shortening and lengthening reduces the effect of active shortening on the amount of force enhancement. If titin contributes to force enhancement (Herzog and Leonard, 2000; Jones et al., 2016; Nishikawa, 2016; Nishikawa, 2020; Shalabi et al., 2017), then titin force must change during active shortening and during the pause between shortening and lengthening.

Assuming that titin functions as a linear spring, its force can be changed by adjusting equilibrium length. The winding-filament hypothesis developed by Nishikawa et al., (2012) predicts changes in titin equilibrium length with increasing cross-bridge force. In the winding-filament hypothesis, strokes of cross bridges rotate actin filaments along their longitudinal axis, based on actin's double helix structure, and this rotation causes titin to be wound upon actin filaments. In particular, an increase in cross bridge force can decrease titin equilibrium length by longitudinally rotating the actin filament (Nishikawa et al., 2012). This hypothesis can explain the reduced effect of shortening on the amount of force enhancement during isometric force redevelopment. When cross-bridge force recovers during isometric force redevelopment, titin equilibrium length would be reduced by titin winding upon actin filaments. During the redevelopment period, the relative contributions of titin equilibrium length and strain to titin force would depend on the initial titin state and cross-bridge force following active shortening. The different contributions might result in different slopes of the relationship between F_{ISO} and k_m because titin stiffness can only affect k_m, but not titin strain.

In conclusion, we found different ratios of k_m to F_{ISO} during isometric force redevelopment following active shortening at different velocities. The greater k_m caused by active shortening can potentially be explained by weakly-bound cross bridges that contribute to k_m but not force. However, the weakly-bound cross-bridge hypothesis is not compatible with

the reduced slope at the slower active shortening velocity or the linear slope between k_m and F_{ISO} during isometric force redevelopment. To explain these observations, an alternative hypothesis is needed. One alternative hypothesis is that titin stiffness changes during active shortening and isometric force redevelopment. The winding filament hypothesis (Nishikawa et al., 2012) provides a plausible mechanism for how titin stiffness is modulated by cross-bridge forces. However, since titin is unobservable due to its small (~4 nm) diameter (Maruyama et al., 1984; Trinick et al., 1984; Wang et al., 1984), direct evidence supporting the winding filament hypothesis is elusive. In the absence of better techniques for observing sarcomere and protein structure during dynamic contractions, developing models that account for changes in muscle stiffness during shortening seems to be essential to further the understanding of muscle mechanics in dynamic experiments with time-varying muscle length and velocity.

Chapter 4. Titin clutch model

4.1 Background

As muscle is the only organ that produces active force, individual muscle force can provide considerable insights into human biomechanics and motor control. However, individual muscle force is only rarely measured due to methodological difficulty. Though joint torque can be quantified using dynamometer equipment (Forrester et al., 2011; Yeadon et al., 2006) or be estimated using inverse dynamics with joint kinematics and ground reaction force (Delp et al., 2007; Kuo, 1998), the issue of assigning joint torque to different muscles that cross the same joint is not easily solved (Hug et al., 2015). Some previous studies have used physiological cross-sectional area or electromyography when assigning torque to muscles (Dick et al., 2016; Maganaris and Paul, 1999), but the accuracy of these approaches remains unknown. Individual muscle force can be measured directly with invasive methods such as optic fibers or transducer buckles applied directly to the tendon (Finni et al., 1998; Hahs and Stiles, 1989). However, these highly invasive methods are not easily applicable and are only rarely used. Simulation of muscle force using muscle models is one alternative way to estimate individual muscle force.

Hill-type models are most commonly used to estimate individual muscle force due to its simplicity (Lloyd and Besier, 2003). The Hill model predicts muscle force based on activation dynamics, isometric force length and isotonic force velocity relationship (Dick et al., 2017). Although the Hill model has the advantage of being relatively simple, the application is increasingly limited. Hill-type models fail to explain the length dependence of activation dynamics (Shue and Crago, 1998) or the history dependence of muscle force (Perreault et al.,

2003; Sandercock and Heckman, 1997; Scovil and Ronsky, 2006). That is, the Hill model predicts the equivalent force at any given same length and activation. The inability of the Hill model to predict variable force depending on length history results in inaccurate predictability of *in vivo* muscle force predictions. For example, this model gives a mean r^2 value of 0.54 for human medial gastrocnemius during cycling (Dick et al., 2017) and the range of r^2 was 0.26 to 0.51 for goat medial gastrocnemius during treadmill walking, trotting and galloping (Lee et al., 2013). These results suggest that alternative muscle models are needed for *in vivo* conditions.

Recent studies have suggested that the tunable viscoelastic property of the giant titin protein may explain the history dependence of muscle force (Nishikawa, 2020). Titin viscoelasticity depends on activation due to calcium-dependent binding of the N2A domain of titin to actin (Dutta et al., 2018). The binding effect is to remove the compliant proximal Ig domain in the active state, which increases titin stiffness. Tunable titin stiffness modulates titin force. Considering the parallel connection between titin and cross bridges (Herzog, 2018), the modulated titin force directly influences muscle force. Indeed, from stretch amplitude-dependent residual force enhancement (Bullimore et al., 2007; Edman et al., 1978; Edman et al., 1982; Hisey et al., 2009), it can be inferred that the length of muscle upon activation is essential to determine titin force. The variable response of titin to activation and length history can explain the history-dependence of muscle force. However, it has rarely been investigated how the titin protein adjusts to changes in force and length once binding to actin occurs, because titin is unobservable due to its small (~4 nm) diameter (Maruyama et al., 1984; Trinick et al., 1984; Wang et al., 1984).

Due to the in series as well as in parallel connection between titin and cross bridges, the titin force should be the same as the cross-bridge force (Herzog, 2018). According to the

winding filament hypothesis (WFH) developed Nishikawa et al. (2012), the effects of titin-actin interactions is to maintain the balance of force between cross bridge and titin. In the WFH, strokes of cross bridges rotate an actin filament along its longitudinal axis based on actin's double helix structure, and this rotation causes titin to be wound upon actin filaments. The increase in cross-bridge force can change titin equilibrium length by modulating the longitudinal rotation of the actin filament (Nishikawa et al., 2012).

The titin clutch model (TCM) was developed with a titin element that wraps around a pully representing the actin filament (Tahir et al., 2018). The titin clutch model consists of three subunits representing the contractile element, the titin element, and the series elastic element. The pulley connects the titin element to the contractile element in series and parallel. The history-dependent pulley position should affect the response of the model to activation, which allows for predicting history-dependent forces. Additionally, activation-dependent parameters were added to the damper in the contractile element and the spring and the damper in the titin element to implement the force velocity relationship scaled to the level of activation (Chow and Darling, 1999) and titin binding to actin in the presence of Ca^{2+} (Dutta et al., 2018).

In this study, we aimed to test the ability of TCM to predict history-dependent muscle force. To investigate the effects of the pulley and the activation-dependent mechanical properties on the accuracy of predicted force, we developed five models: 1) the titin clutch model with activation-dependent mechanical properties and a pulley (TCM); 2) TCM with no activation-dependent mechanical properties (TCM_{noAct}); 3) TCM with no pulley (TCM_{noPll}); 4) TCM with neither activation-dependent parameters nor pulley ($TCM_{noPllAct}$); and 5) a Hill model with third order activation dynamics (Wakeling et al., 2021). All models were used to simulate *in situ* data measured during work loops with length perturbations of cockroach leg

muscle (Libby et al., 2020). We hypothesized that: 1) the TCM will predict muscle force more accurately than the Hill model; 2) the TCM models with the pulley will predict muscle force more accurately than models with no pulley (TCM vs. TCMnoPll & TCM_{noAct} vs. $TCM_{noPllAct}$); and 3) the TCM models with activation-dependent parameters will predict muscle force more accurately than models with no activation-dependent parameters (TCM vs. TCM_{noAct} & TCM_{noPll} vs. $TCM_{noPllAct}$).

4.2 Materials and Methods

4.2.1 Data for models

We used data from a study of cockroaches (Libby et al., 2020) during sinusoidal work loops at six different frequencies (1, 3, 5, 8, 10 and 12 Hz) with length perturbations. The target muscle was the ventral femoral extensor of the middle leg (muscle 137). Instead of isolating the muscle from the limbs, intact joint work loops were performed. A muscle ergometer located at the coxa-femur joint controlled joint trajectories and measured force simultaneously. The target muscle was activated via implanted bipolar silver wire electrodes.

The data used for simulations in the present study included 24 trials (four types at six frequencies). The types included length perturbations occurring shortening or at lengthening phase and whether the muscle was activated or not before the length perturbations. In the active type, muscles were activated 25 ms before length perturbations and activation ended at the start of length perturbations. Length perturbations always occurred at the same muscle length and velocity, and the shape was a half sinusoidal curve at 1000 Hz. The amplitude of length perturbations was set to equal to the stride amplitude. Six trials were randomly chosen to train the models and the trained model was tested on the other 18 trials. Muscle force was normalized to the maximal isometric force (P_0) and length was normalized to the optimal length (L_0) that produced the maximal isometric force. Stimulation also was normalized to the peak voltage. In this study, relative force (% P_0), relative length (% L_0) and relative stimulation were used to validate the muscle models.

4.2.2 Titin clutch muscle models

The titin clutch model (TCM) consists of a contractile element, a titin spring and

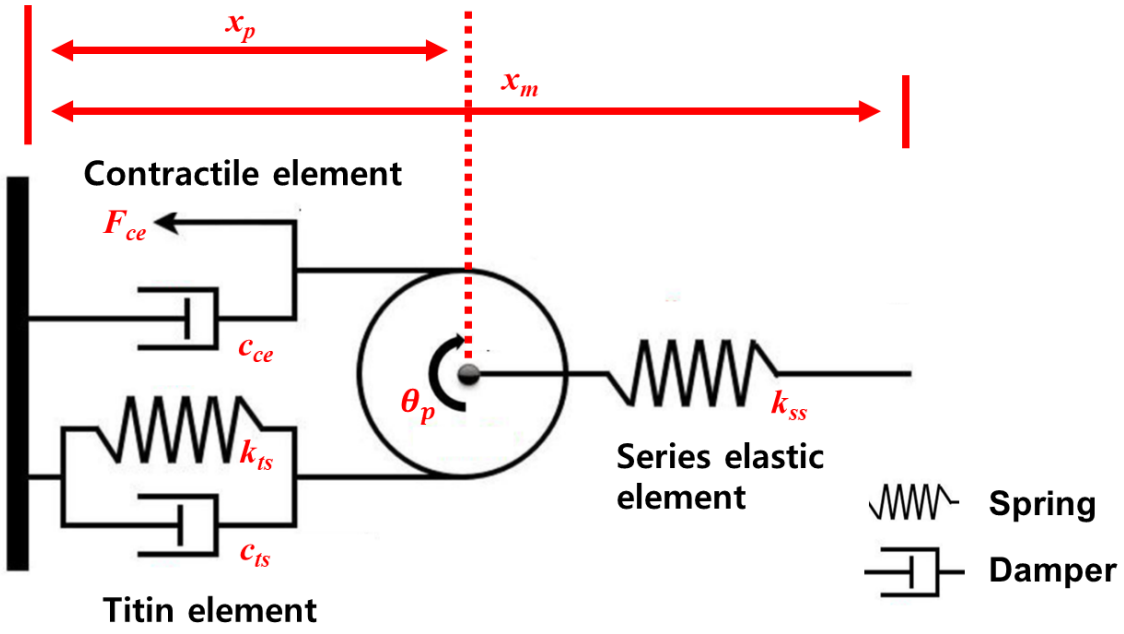

Figure 4.1: Schematic of the titin clutch model. In the titin clutch model, the contractile element (*ce*) is a nonlinear damped motor. m_p, r_p and $\boldsymbol{\theta_p}$ represent mass, radius, and angle of the pulley. When *ce* force increases, the pulley rotates in the counter-clockwise direction. The series elastic element represents tendon, aponeurosis, and extracellular matrix. A spring and damper represent the viscoelastic properties of titin with spring constant k_{ts} and damping coefficient c_{ts}.

damper, a pulley, and a series elastic element. x_m and x_p represent the whole muscle length and the distance between z-disc and the center of the pulley, respectively. θ_p shows the angle of the pulley (Fig. 4.1). The pulley reflects the behavior of titin in the winding filament hypothesis (Nishikawa et al., 2012), in which the titin filament winds around actin filaments depending on the rotation of the actin filament along the longitudinal axis by the cross bridges. The pulley is frictionless and in a no-slip condition and has two degree of freedom (DOF), rotation and translation. The rotational acceleration of the pulley can be written as:

$$J_p\ddot{\theta}_p = r(F_c - F_t) - TQ_p, \quad (1)$$

where r, J_p and θ_p are the radius, the inertia, and the angle of the pulley, respectively. F_c, F_t and TQ_p represent the contractile element force, titin force, and pulley recoil torque. The

transitional acceleration of the pulley is given by:

$$m_p\ddot{x}_p = F_{ss} - (F_t + F_c), \quad (2)$$

where m_p is the mass of the pulley and x_p is the change in pulley position. Parameter values for m_p and r were set at 10^{-3} P_0 and 1 L_0, respectively. The pulley moment of inertia was calculated based on m_p and r ($J = m_p r^2$).

The contractile element is composed of a force generator ib parallel with a damper. Force developed by the force generator is determined by the level of activation and whole muscle length. F_{ce} is given by:

$$F_{ce} = \exp\left(-\frac{(x_m-1)^2}{\gamma}\right) \times (Act \times Act_{scale}), \quad (3)$$

where x_m is relative muscle length, Act represents the level of activation and Act_{scale} is a parameter that scales activation to force. In this study, γ was set at 0.45 to represent a physiologically relevant force-length relationship (Gordon et al., 1966; Thelen, 2003). The damping force, F_{cd}, is determined by damping coefficient, c_{ce}, and the change in velocity of the contractile element, $\dot{x}_{ce}$ (Fig. 1). F_{cd} is given by:

$$\dot{x}_{ce} = \dot{x}_p - r\dot{\theta}_p \quad (4)$$

$$F_{cd} = c_{ce} \times \dot{x}_{ce}, \quad (5)$$

$$c_{ce} = c_1 \times e^{c_2 \cdot Act \cdot |\dot{x}_p|}, \quad (6)$$

where $\dot{x}_{ce}$ is the rate of change in the contractile element, Act represents the level of activation, $\dot{\theta}_p$ is the rate of change in the pulley angle, and c_1 and c_2 are constant parameters. Because the force generator is in parallel with the damper, F_c is determined by the sum:

$$F_c = F_{ce} + F_{cd}. \quad (7)$$

The titin element consists of a spring and damper. As titin is wound around the pulley, the whole titin segment is divided into two parts: free titin and bound titin. Since the model

assumes that the pulley is frictionless in no-slip condition and the wound part of titin is firmly bound to the pulley, only the free titin contributes to the mechanical properties of the model.

Changes of the equilibrium length of the free titin segment can be modeled using a differential equation. When the pulley rotates by a small angle $\Delta\theta$, the amount of the wrapped portion around the pulley is $r{\cdot}\Delta\theta$. The rate of change of the equilibrium length is:

$$\dot{l_{eq}} = -l_{eq} \cdot \frac{r\theta_p}{x_p}, \tag{8}$$

where l_{eq} represents the equilibrium length of the titin spring, r, θ_p are the radius and angle of the pulley, respectively, and x_p is the length of free titin segment:

$$l_{eqNew} = l_{eqOld} + \dot{l_{eqOld}}, \tag{9}$$

$$k_{tsNew} = k_{tsOld} \times \frac{l_{eqOld}}{l_{eqNew}}, \tag{10}$$

where l_{eqNew} and l_{eqOld} represent the equilibrium length after and before rotation of the pulley. Titin spring stiffness (k_{ts}) is affected by changes in equilibrium length of the free titin segment and is determined by the ratio of l_{eqNew} to l_{eqOld}.

It has been suggested that titin increases its stiffness by binding of N2A titin to actin in the presence of Ca^{2+} (Dutta et al., 2018). Since the probability of titin binding to actin depends on the concentration of Ca^{2+}, it is likely that titin stiffness increases with increasing activation. Thus, this model assumes that the activation level determines the relative contribution of active and passive titin stiffness:

$$k_{ts} = (1 - Act) \times k_{tsPass} + Act \times k_{tsNew}, \tag{11}$$

Titin spring force is given by:

$$F_{ts} = k_{ts} \cdot x_p, \tag{12}$$

The titin damper has a velocity-dependent damping coefficient. The damping coefficient is:

$$c_{ts} = (1 - Act) \times c_{tsPass} + Act \times c_{tsAct}, \quad (13)$$

where c_{tsPass} and c_{tsAct} represent the damping coefficient in passive and active state, respectively. Titin damping force is given by:

$$F_{td} = c_{ts} \times (\dot{x}_p + \dot{\theta}_p), \quad (14)$$

As the titin spring is in parallel with the titin damper, the titin force is the sum of those forces:

$$F_t = F_{ts} + F_{td}. \quad (15)$$

In the model, a torsion spring represents alpha-actinin in the Z-disk. In the cross-sectional view of the Z-disk, the lattice structure of alpha-actinin changes from square to the basket-weave when muscles develop force (Oda and Yanagisawa, 2020). In the WFH, actin's longitudinal rotation developed by cross-bridge axial torque causes the change in the lattice structure. The torsional strain of alpha-actinin in the Z-disk produces a recoil torque to return the thin filament toward its original structure, which results in unwinding of titin (Nishikawa et al., 2012). To model the unwinding force, the model has a torsion spring in the pulley. The spring torque is given by:

$$TQ_p = k_p \times \theta_p, \quad (16)$$

The series elastic element force is represented as a constant stiffness (k_{ss}) multiplied by the distance between whole length of muscle (x_m) and the pulley position (x_p) (Fig. 1):

$$F_{ss} = k_{ss} \times (x_m - x_p). \quad (17)$$

4.2.3 TCM sub-models

The current version of the titin clutch model has two unique properties: a pulley and activation-dependent parameters. To evaluate the effect of these properties, we developed several models based on the TCM with no pulley, no activation-dependent parameters, or neither. First, we developed the titin clutch model with no pulley (TCM_{noPll}). Because the model

has no pulley, it does not include pulley rotation:

$$F_{ss} = F_c + F_t, \tag{18}$$

where, F_{ss} is series elastic force, F_c is the force from the contractile element, F_t is the force from the titin element. The velocity of the contractile element is:

$$\dot{x}_{ce} = \frac{F_{ss} - (F_{ce} + F_t)}{c_{ce}} \tag{19}$$

where, $\dot{x}_{ce}$ is the velocity of the contractile element, F_{ce} represents force from the force generator in the contractile element and c_{ce} is the coefficient for the damper in the contractile element.

To investigate the effect of activation-dependent parameters, the model without activation-dependent parameters (TCM_{noAct}) was developed based on the TCM. In the model, c_{ce}, k_{ts}, and k_{td} were no longer affected by the level of activation. The model with neither activation dependent parameters nor the pulley ($TCM_{noPllAct}$) was developed with constant c_{ce}, k_{ts}, and k_{td} based on TCM_{noPll}.

4.2.4 Hill-type muscle model

A Hill-type model with third order activation dynamics based on Wakeling et al., (2021) was simulated. Muscle forces F_m were calculated as follows:

$$F_m = F_0 \left[\hat{a}(t)\hat{F}_a(\hat{l})\hat{F}_v\left(\frac{d\hat{l}}{dt}\right) + \hat{F}_p(\hat{l}) \right], \tag{20}$$

Where, F_0 represents maximal isometric force, $\hat{F}_a$ and $\hat{F}_v$ represent the active force length relationship and the force velocity relationship, respectively, and $\hat{F}_p$ is the passive force of the parallel elastic element. $\hat{l}$ was normalized muscle length. $\hat{F}_a$ and $\hat{F}_p$ were modeled as exponential functions, and $\hat{F}_v$ was expressed as a piecewise function to implement the

different curvature of each contraction mode. In an active $\hat{F}_a(\hat{l})$ model, the active force length relationship was represented using three parameters (*r*, *s* and *w*),

$$\hat{F}_a(\hat{l}) = e^{-\left|\frac{\hat{l}^w - 1}{s}\right|^r} \tag{21}$$

where *r*, *s*, and *w* determine roundness, width, and skewness of the force length relationship, respectively. Passive force is computed as

$$\hat{F}_p(\hat{l}) = e^{(c_1 + c_2\hat{l})} \tag{22}$$

where c_1 and c_2 are experimental coefficients.

The force velocity relationship was composed of three parts depending on muscle velocity,

$$\hat{F}_v\left(\frac{d\hat{l}}{dt}\right) = 0 \; for \; \frac{d\hat{l}}{dt} < -1 \tag{23}$$

$$\hat{F}_v\left(\frac{d\hat{l}}{dt}\right) = \frac{1 + (\frac{d\hat{l}}{dt})\frac{1}{v_0}}{1 - (\frac{d\hat{l}}{dt})\frac{1}{kv_0}} \; for -1 \leq \frac{d\hat{l}}{dt} < 0 \tag{24}$$

$$\hat{F}_v\left(\frac{d\hat{l}}{dt}\right) = 1.5 - \frac{0.5\left[1 - \left(\frac{d\hat{l}}{dt}\right)\frac{1}{v_0}\right]}{1 + 7.56\left(\frac{d\hat{l}}{dt}\right)\frac{1}{kv_0}} \; for \; \frac{d\hat{l}}{dt} \geq 0 \tag{25}$$

where v_0 represents the maximum contraction velocity, and *k* determines the curvature of the force velocity relationship. For the eccentric contraction, parameters were taken from Wakeling et al. 2021.

$\hat{a}(t)$ used three coupled differential equations to convert from the excitation to an activation signal (Lee et al., 2013). The excitation was taken as stimulation from the cockroach data.

4.2.5 Model parameter optimization and numerical integration

The second order ordinary differential equation (ODE) in TCM and TCM_{noAct} and the first order ODE in TCM_{noPll} and $TCM_{noPllAct}$ were numerically integrated using ODE15s function in MATLAB (Mathworks, R2020a, Natick, MA).

TCM had nine free parameters including the series spring coefficient (k_{ss}), two titin spring coefficients (k_{tsPass} & k_{tsAct}), two titin damper constants (c_{tsPass} & c_{tsAct}), two contractile element damping constants (c_1 & c_2), torsion spring constant (k_p) and the activation scale factor (Act_{scale}). In TCM sub-models, TCM_{noAct} had seven free parameters (no k_{tsPass} or C_{tsPass}). The number of parameters in TCM_{noPll} was eight (no k_p). $TCM_{noPllAct}$ had only six free parameters after removing the pulley (k_p) and activation-dependent parameters (k_{tsPass} and c_{tsPass}). The free parameters were optimized for the highest r^2 between the predicted force and the measured force in training data (6 trials) using the Particle Swarm function in MATLAB.

In the Hill model, seven free parameters for the force-velocity and the active and passive force-length relationships, and eight free parameters for the third order activation dynamics were optimized to obtain the best r^2 value between the predicted and measured force. The initial values of the seven free parameters describing the active and passive force-length relationship and the force-velocity relationship were taken from a previous study of cockroaches (Ahn et al., 2006). We extracted data for the force-velocity and the force-length relationship from Ahn et al. (2006) and then performed curve fitting to obtain the seven free parameters. The upper and lower bounds of the parameters set to 95% confidence interval for the curve fitting. Additionally, the eight parameters related to third order activation dynamics were optimized without any considerations of physiological relevance. Particle Swarm function in MATLAB was used to obtain the best parameter set with the highest r^2 value in training data.

4.2.6 Statistical analysis

The coefficient of determination (r^2) and the root mean square error (*RMSE*) were used to characterize differences between predicted and experimentally measured forces. To test hypotheses 1, 2, and 3, a one-way ANOVA was used to determine r^2 and *RMSE* differences among muscle models in the training and the test set. When significant differences existed, Tukey's honestly significant difference (HSD) test was used to determine where the differences occurred. Additionally, we calculated r^2 to evaluate the relationship between predicted peak forces and measured peak forces during length perturbations in the training and the test data. The level of significance was set at $p < 0.05$. Values in the text are reported as mean ± standard deviation.

4.3 Results

We developed and tested five models: 1) a titin-clutch model with activation-dependent parameters and a pulley (TCM); 2) a titin-clutch model without activation-dependent parameters (TCM_{noAct}); 3) a titin-clutch model with no pulley (TCM_{noPll}); 4) a titin-clutch model with neither activation-dependent parameters nor pulley ($TCM_{noPllAct}$); and 5) a Hill model with third-order activation dynamics. The parameter sets of all models for the highest r^2 between predicted and measured force were obtained using the training data (six of 24 trials). All models predicted muscle force in the test data (18 trials of 24 trials) with the obtained parameter set (Fig. 4.2). Coefficient of determination (r^2) and root mean squared error (*RMSE*) were calculated to evaluate the accuracy of predicted muscle forces compared to experimentally measured muscle forces.

Table 4.1: Results of *post-hoc* tests showing the difference of mean r^2 and *RMSE* among the muscle models

	Training		Test	
	r^2	*RMSE*	r^2	*RMSE*
TCM	0.77 ± 0.08[b]	12.35 ± 2.57	0.82 ± 0.07[c]	11.80 ± 2.28
TCM_{noAct}	0.79 ± 0.07[b]	11.27 ± 1.04	0.82 ± 0.07[c]	10.43 ± 2.57
TCM_{noPll}	0.75 ± 0.09[b]	15.41 ± 2.14	0.80 ± 0.08[c]	14.27 ± 3.95
$TCM_{noPllAct}$	0.76 ± 0.08[b]	14.08 ± 1.98	0.80 ± 0.07[c]	12.90 ± 4.21
Hill	0.43 ± 0.26	16.27 ± 6.26	0.52 ± 0.26	13.80 ± 6.90

[a] significantly different from Hill ($p < 0.05$)

[b] significantly different from Hill ($p < 0.01$)

[c] significantly different from Hill ($p < 0.001$)

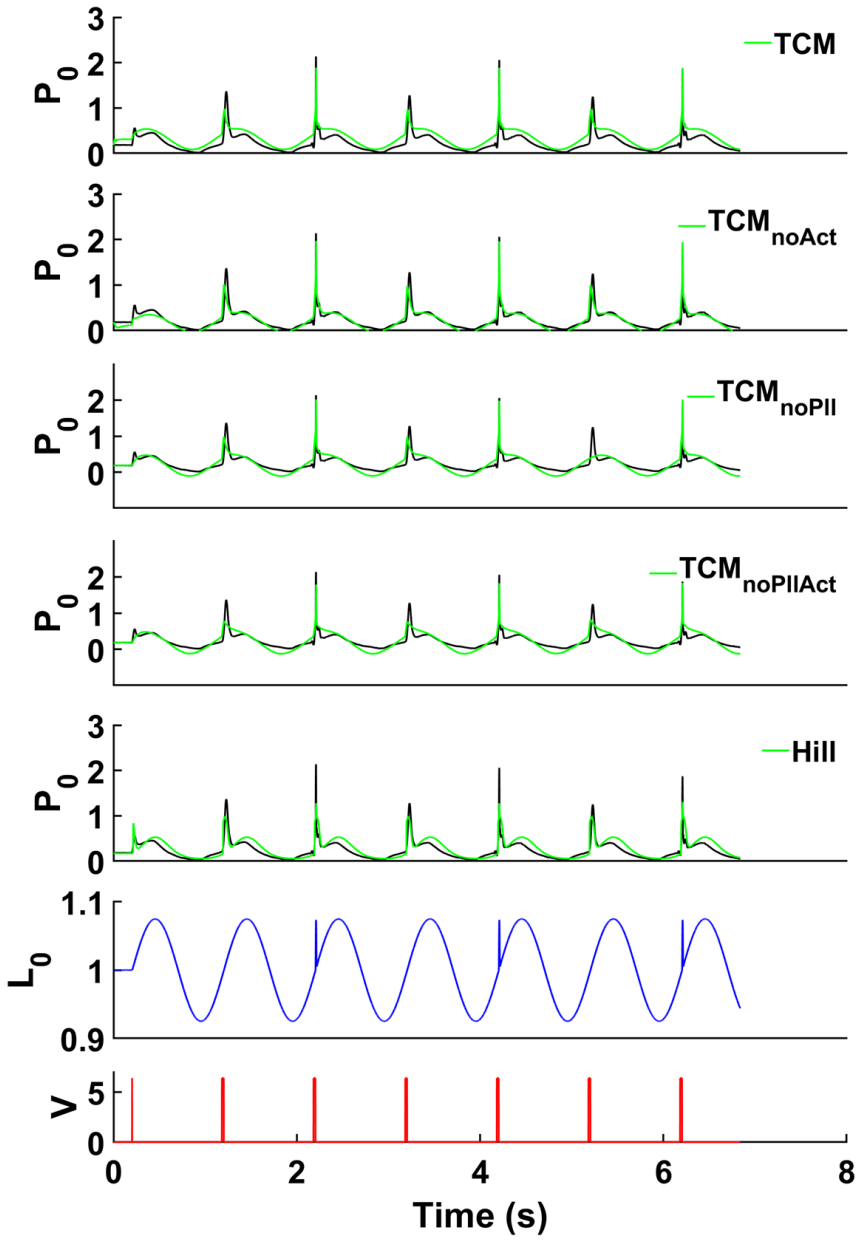

Figure 4.2: Cockroach ventral femoral extensor muscle length, stimulation, force, and predicted forces. Forces were predicted from the muscle models (green) and measured from a muscle ergometer (black). Muscle length was measured by the muscle ergometer (blue). The muscle was stimulated via implanted electrodes (red line).

There were significant differences in r^2 among muscle models in the training (F = 7.08, $p < 0.001$) and the test data (F = 16.72, $p < 0.001$). In the training data, values of r^2 for TCM ($r^2 = 0.77 \pm 0.08$), TCM_{noAct} ($r^2 = 0.79 \pm 0.07$), TCM_{noPll} ($r^2 = 0.75 \pm 0.09$), and $TCM_{noPllAct}$ ($r^2 = 0.76 \pm 0.08$) were larger than for the Hill model ($r^2 = 0.43 \pm 0.26$) (HSD, $p < 0.01$). In the test data, values of r^2 for TCM ($r^2 = 0.82 \pm 0.07$), TCM_{noAct} ($r^2 = 0.82 \pm 0.07$), TCM_{noPll} ($r^2 = 0.80 \pm 0.08$) and $TCM_{noPllAct}$ ($r^2 = 0.80 \pm 0.07$) did not differ significantly from each other, but r^2 was larger than for the Hill model ($r^2 = 0.52 \pm 0.26$) (HSD, $p < 0.001$) (Table 4.1 and Fig. 4.3A and B).

The *RMSE* values did not differ significantly among muscle models in the training (F = 2.34, $p = 0.083$) and test data (F = 2.34, $p = 0.062$). In the training data, *RMSE* for the Hill model (*RMSE* = 16.27 ± 6.26), TCM (*RMSE* = 12.35 ± 2.57), TCM_{noAct} (*RMSE* = 11.27 ± 1.04), TCM_{noPll} (*RMSE* = 15.41 ± 2.14), and $TCM_{noPllAct}$ (*RMSE* = 14.08 ± 1.98) were not significantly different from each other. In the test data, the Hill model (*RMSE* = 13.80 ± 6.90) did not yield significantly different *RMSE* from TCM (*RMSE* = 17.70 ± 9.35), TCM_{noAct} (*RMSE* = 17.70 ± 9.35), TCM_{noPll} (*RMSE* = 14.27 ± 3.95), and $TCM_{noPllAct}$ (*RMSE* = 17.70 ± 9.35). *RMSE* for TCM, TCM_{noAct}, TCM_{noPll}, and $TCM_{noPllAct}$ also did not differ significantly from each other (Table 4.1 and Fig. 4.3C and D).

Although r^2 and *RMSE* for an entire trial did not differ among TCM, TCM_{noAct}, TCM_{noPll}, and $TCM_{noPllAct}$ in the training and test data, the models showed differential ability to predict peak force during the length perturbation. TCM_{noAct} predicted peak muscle force the best ($r^2 = 0.80$), and TCM ($r^2 = 0.75$) and the Hill model ($r^2 = 0.72$). predicted peak force better than TCM_{noPll} ($r^2 = 0.45$) and $TCM_{noPllAct}$ ($r^2 = 0.54$) (Fig. 4.4).

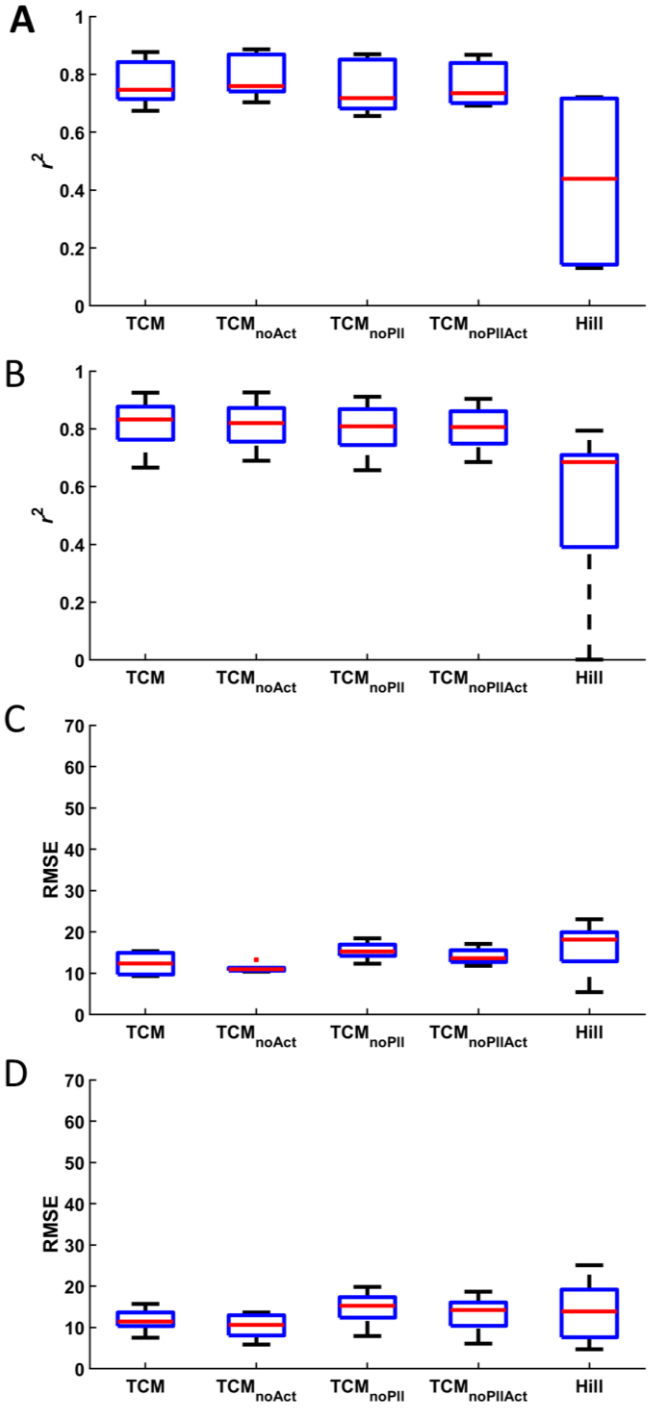

Figure 4.3: Summary box plots (r^2 and RMSE) for the training set (A, C) and the test set (B, D). Horizontal line (red) dividing upper and lower half of boxplot represents median, and upper and lower boxplot depict 75th and 25th percentile, respectively. Upper whisker represents 90th percentile and lower whisker shows 10th percentile.

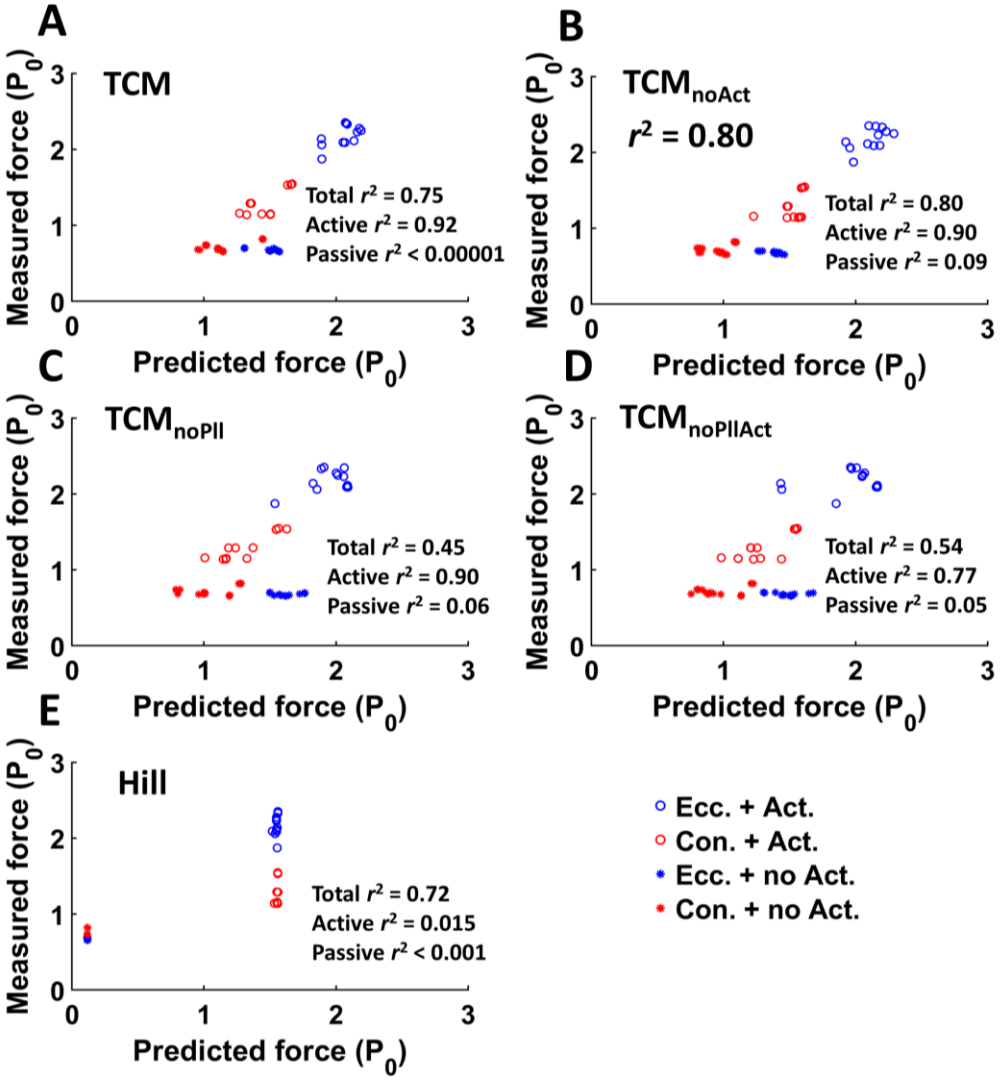

Figure 4.4: The relationship between predicted and measured peak force during length perturbations. The cockroach data included four types of trials: 1) Ecc. + Act, the length perturbation occurs during lengthening with stimulation (blue circle); 2) Con. + Act, the length perturbation occurs during shortening with stimulation (red circle); 3) Ecc. + no Act, the length perturbation occurs during lengthening with no stimulation (blue star); and 4) Con. + no Act, the length perturbation occurs during shortening with no stimulation (red star). There was no difference in measured force between the passive lengthening and the shortening trials, but peak forces were greater during active lengthening than during active shortening. r^2 was calculated between measured and predicted peak forces. The titin clutch model (TCM), the titin clutch model with no activation dependent parameters (TCM_{noAct}), and the Hill model predicted peak forces more accurately than the model with no pulley (TCM_{noPll}) and the model with neither pulley nor activation-dependent parameters ($TCM_{noPllAct}$).

4.4 Discussion

The aim of this study was to incorporate activation-dependent mechanical properties of titin (Nishikawa et al., 2012) and a contractile element into a testable a titin-clutch model (TCM) inspired by titin-actin interactions (Dutta et al., 2018). The TCM is composed of three elements: a contractile element, a titin element, and a series elastic element. A pulley was added to connect and emulate the titin element to the contractile element. A spring and damper in the contractile and titin elements have an activation-dependent coefficient to implement variable force-velocity relationship scaled by activation (Chow and Darling, 1999) and binding of titin to actin in the presence of Ca^{2+} (Dutta et al., 2018). To explore whether the pulley and the activation-dependent mechanical properties improve the accuracy of the predictions of force, the accuracy of predicted force was compared among four muscle models: 1) TCM with no activation-dependent mechanical properties (TCM_{noAct}), 2) TCM with no pulley (TCM_{noPll}), 3) TCM with neither pulley and activation-dependent mechanical properties ($TCM_{noPllAct}$), and 4) the Hill model. Data collected *in situ* during sinusoidal work loops with length perturbations of cockroach leg muscle was used to test the muscle models.

There was no significant decrease in the accuracy of force predictions (r^2 and *RMSE*) between the training and the test data. This finding suggests that overfitting did not occur in any models. In the training and the test data, the *RMSE* values for all models did not significantly differ from each other, but the r^2 values for TCM, TCM_{noAct}, TCM_{noPll}, and $TCM_{noPllAct}$ were significantly higher than for the Hill model.

4.4.1 Comparison of the titin-clutch model and Hill models

TCM ($r^2 = 0.77 \pm 0.08$), TCM_{noAct} ($r^2 = 0.79 \pm 0.07$), TCM_{noPll} ($r^2 = 0.75 \pm 0.09$), and $TCM_{noPllAct}$ ($r^2 = 0.76 \pm 0.08$) yielded higher r^2 values than the Hill model ($r^2 = 0.43 \pm 0.26$) in

the training data. Also, in the test data, the r^2 values for TCM ($r^2 = 0.82 \pm 0.07$), TCM_{noAct} ($r^2 = 0.82 \pm 0.07$), TCM_{noPll} ($r^2 = 0.80 \pm 0.07$), and $TCM_{noPllAct}$ ($r^2 = 0.80 \pm 0.08$) were significantly higher than for the Hill model ($r^2 = 0.52 \pm 0.26$). In the present study, the parameters describing the force-velocity (FVR) and the force-length relationship (FLR) were estimated from muscle 178 data of the cockroach in a previous study (Ahn et al., 2006), because the data used in the present study was collected from cockroach leg muscle 137 (Libby et al., 2020). Although the previous studies used the same species of the cockroach (*Blaberus discoidalis*), muscle was different. A previous study demonstrates the subject-specific data improves the accuracy of forces predicted using the Hill model (Gerus et al., 2012; Gerus et al., 2015; Wakeling et al., 2021). The parameters estimated from the subject-specific data would lead to a better model prediction of muscle force.

The Hill model yielded similar r^2 values for peak muscle force during length perturbations (Hill $r^2 = 0.72$, TCM $r^2 = 0.75$), although Hill model had lower accuracy in predicting muscle force for an entire trial than the TCM (Table 4.1). In the cockroach data, length perturbations were performed at the same muscle length and velocity. Passive peak forces during length perturbations were almost constant regardless of strain history (Fig. 4.4, blue and red star), but active peak forces were affected by strain history (Fig. 4.4, blue and red circle). The Hill model predicted relatively constant passive peak forces very accurately (Fig. 4.4E, blue and red star), but failed to predict the history-dependent active peak forces, showing the relatively constant active peak forces like passive peak forces (Fig. 4.4E, blue and red circle, $r^2 = 0.015$). These results suggest that the Hill model does not explain the history-dependence of force since the Hill model produces same force at same length and activation. In contrast, the TCM showed the ability to accurately predict the history dependent active peak forces (Fig.

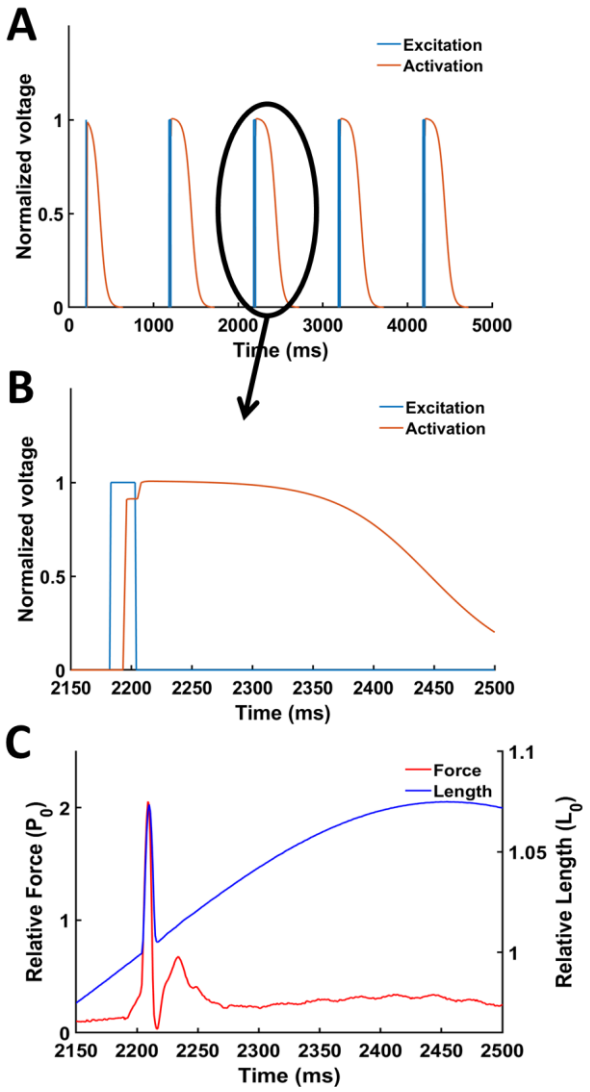

Figure 4.5: Predicted relative muscle activation (red) from third order activation dynamics and stimulation intensity (blue) (A & B) compared to measured force (red) and length (blue) (C). The third-order activation dynamics convert excitation to force. The parameters of the activation dynamics were optimized for the best r^2 value between predicted force and measured force. One effect of the activation dynamics is to offset the delay between the onset of stimulation and the onset of force by shifting predicted activation later in time.

4.4A, blue and red circle, $r^2 = 0.92$).

The TCM does not include FVR, while the Hill model uses the isotonic FVR to represent changes in force depending on velocity. Instead, the TCM includes a nonlinear

damper in parallel with the contractile element to explain the nonlinear decrease or increase in force with velocity. Even without FVR, the TCM predicted muscle force in an entire trial and peak muscle forces during length perturbations more accurately than the Hill model. Furthermore, the nonlinear damper accounts for the delay between stimulation onset (Fig. 4.5B, blue) and force onset (Fig. 4.5C, red) without any changes in phase of stimulation.

In the Hill model, the third-order activation dynamics shifted the predicted activation toward later times to account for the delay between the onset of stimulation and the onset of force (Fig. 4.5). The role of activation dynamics in the muscle model is to capture the charge and discharge rates of the muscle membrane and the electromehcanical delay (Seth et al., 2011; Zajac, 1989). Although the activation dynamics predicted the delay accurately in cockroach data (Fig. 4.5B and C), the relaxation of activation is too long (> 350 ms) and the shape of predicted activation is not typical for activation (Fig. 4.5B). That is, the predicted activation is not physiologically relevant. Unlike cockroach data, the level of activation and the delay are variable during *in vivo* movements (Daley and Biewener, 2011). The activation dynamics should be explored whether they predict activation reasonably in *in vivo* data.

4.4.2 The effect of the pulley on prediction of muscle force

The effect of the pulley is to maintain a force balance between the contractile and titin elements through rotational movement of the pulley. If the contractile element force increases as the level of activation increases, the pulley rotates in the counterclockwise direction until the titin element force is the same as the contractile element force, or vice versa. In the passive state, the pulley rarely contributes to muscle force since its rotation is minimal due to the absence of force from the contractile element. The cockroach data we simulated in the present study was measured in the passive state except during active length perturbations (Fig. 4.2).

Therefore, the values of r^2 and *RMSE* for an entire trial are not appropriate for evaluating the effect of the pulley on the accuracy of muscle force predictions.

TCM models with a pulley (TCM and TCM_{noAct}) predicted peak muscle force during length perturbations better than the same models with no pulley (TCM_{noPll} and $TCM_{noPllAct}$) (Fig. 4.4), although r^2 and *RMSE* did not differ significantly for an entire trial (Table 4.1 and Fig. 4.3). Whereas peak forces in the active state varied depending on strain history (Fig. 4.4, blue and red circle), peak forces in the passive state were nearly constant regardless of strain history (Fig. 4.4, blue and red star). When a muscle model responds differently to varying strain history, the model can accurately predict muscle force. In the models with no pulley, the predicted peak forces that occurred during lengthening were higher than during shortening in both the active and the passive case (Fig. 4.4C and D). However, the models with the pulley differently responds to passive length perturbations and active length perturbations. The models predicted peak forces accurately in the active case. Although the predicted peak forces during lengthening were higher than during shortening in the passive case, the pulley reduced the difference of peak forces between lengthening and shortening, compared to the models with no pulley (Fig 4.4A and B). These findings suggest that the effect of the pulley is to control the response of force to length perturbations based on whether muscle is activated or not.

4.4.3 The effect of activation dependent mechanical properties on the prediction of muscle force

We also explored the effects of adding activation-dependent mechanical properties to the TCM model. To implement the force-velocity relationship scaled to activation (Chow and Darling, 1999), the parameter representing activation level was added to an exponential function for the damping coefficient (eq. 6). Additionally, it has been suggested that titin binds

to actin in the presence of Ca^{2+}, which increases its stiffness by removing the compliant tandem Ig domains (Dutta et al., 2018). In the TCM model, the level of activation determines the ratio of passive to active stiffness (eq. 11), and the total titin stiffness is the sum of the passive and active stiffness. The damping coefficient in the titin element is determined in the same way to determine the titin damping (eq. 13).

Activation-dependent mechanical properties were expected to induce different responses to length perturbations between passive and active states. We found no significant differences of r^2 and *RMSE* when activation dependent mechanical properties were added to the TCM models (Table 4.1 and Fig. 4.3). TCM and TCM_{noAct} yielded similar r^2 and *RMSE* values, and r^2 and *RMSE* were not significantly different between TCM_{noPll} and $TCM_{noPllAct}$ (Table 4.1 and Fig. 4.3). Additionally, the activation-dependent mechanical properties did not improve the accuracy of peak muscle force predictions during length perturbations (Fig. 4.4). Instead, values of r^2 for TCM_{noAct} and $TCM_{noPllAct}$ (Fig. 4.4B and D) were higher than for TCM and TCM_{noPll}, respectively (Fig. 4.4A and C). The activation dependent terms had no effects on the predictions of muscle force at least in our results.

The further research seems to be needed to explore whether the effects of activation dependent mechanical properties exist. In the data used in the present study, the amplitude of stimulation was constant throughout all trials and muscle was stimulated for 25ms before length perturbations. The extremely controlled stimulation environment might not be enough to test if the activation dependent properties improve the muscle model.

4.4.4 Limitations

Although the Hill model used the physiologically relevant parameters describing FVR and FLR (Table 4.2), it is unknown whether the parameters for the TCM were within the

physiologically relevant range because the mechanical properties of titin are elusive (Table 4.2). Since titin is unobservable because of its small size (~4nm diameter) (Maruyama et al., 1984; Trinick et al., 1984; Wang et al., 1984), it is not possible for observing sarcomere and protein structure under dynamic conditions. If the physiologically relevant parameters describing the mechanical properties of titin were used to run the model, it may enhance our understanding of how titin behaves under dynamic conditions.

The data we used in the present study had very limited stimulus. Of course, using the data, we were able to test whether the muscle models accurately predict muscle force at different frequencies and to explore the ability to predict the history-dependence of peak muscle force in the passive and the active state. But the data measured with variable level of activation would be useful to investigate the effects of the pulley and the activation dependent mechanical properties.

4.4.5 Conclusion

This simulation study demonstrates that the TCM predicted force for *in situ* cockroach leg muscle during work loops more accurately than the Hill model. Only the TCM models were able to predict variable muscle force as a function of strain history. The effect of the pulley between the contractile and titin elements in TCM models enabled different responses to length perturbations between the active and passive state. The absence of history-dependent forces in the Hill model reduced the accuracy of force predictions under dynamic conditions. The Hill model dictates the same force at a given same length, velocity, and activation. To accurately predict muscle force under dynamic conditions, an alternative muscle model is required. We suggest that incorporating a tunable titin spring in muscle models improves force predictions during dynamic length changes.

Chapter 5. Conclusion

In the traditional "text book" muscle viewpoint of "muscle as motor", the attached cross bridge is the fundamental force-producing unit (Gordon et al., 1966; Huxley, 1957; Huxley and Simmons, 1971). The level of activation, length, and velocity of muscle have been regarded as factors that affect the number of attached cross bridge or the force per cross bridge (Buchanan et al., 2004; Dick et al., 2017; Lloyd and Besier, 2003; Seth et al., 2011; Wakeling et al., 2021; Zajac, 1989). Muscle models based on this viewpoint accurately predict individual muscle force in *in vitro* muscle contraction as well as *in vivo* conditions, but have limitations when predicting force in dynamic conditions due to the inability to predict the history-dependence of muscle force (Dick et al., 2017; Lee et al., 2013; Sandercock and Heckman, 1997).

In recent years, it has been increasingly accepted that titin plays a critical role in regulating active muscle force by changing its elastic properties (Hessel et al., 2019; Lindstedt and Nishikawa, 2017). The tunable elastic properties of titin enable prediction of history-dependent muscle forces (Herzog, 2018; Herzog, 2019; Lappin et al., 2006; Monroy et al., 2017; Nishikawa, 2016; Nishikawa, 2020; Nishikawa et al., 2012; Tahir et al., 2020). The "muscle as composite material" viewpoint is based on the tunable elastic properties of titin. Because muscle is an active composite material, muscle force is determined by its mechanical response to externally applied forces (Nishikawa, 2020). This alternative paradigm is expected to simulate muscle force more accurately in dynamic conditions. However, there is a lack of experimental evidence to support this recent alternative hypothesis. Therefore, the aim of this dissertation was to explore the limitations of the traditional muscle viewpoint and to test

predictions of the alternative muscle viewpoint. To achieve this aim, we investigated: 1) how the role of activation changes depending on muscle length history; 2) how length history modulates muscle stiffness in the active state; and 3) whether an alternative muscle model based on titin's tunable viscoelastic properties can predict muscle force more accurately than a Hill-type muscle model based on the traditional muscle viewpoint.

5.1 Specific Aim 1: Decoupling between activation and force

To clarify the role of neural activation and length perturbations in determining muscle force, two protocols were performed. The first protocol evaluated how muscle responds to different levels of activation depending on length history, and the second protocol measured the response of muscle to length perturbations for different length histories. Our findings showed that different length histories induced different muscle viscoelastic properties, which then regulated the contribution of activation and length perturbations to muscle force. As muscle has greater stiffness following active shortening at slow velocity, muscle responds more sensitively to changes in activation and length. The results suggest that muscle viscoelastic properties play an important role in determining the relative contribution of activation or length perturbations to muscle force. Since muscle viscoelastic properties are affected by length history, a muscle model cannot predict muscle force accurately without consideration of strain history. A new alternative muscle viewpoint is required that includes tunable viscoelastic properties.

5.2 Specific Aim 2: Titin as a tunable viscoelastic element in active muscle

Titin is a giant protein that spans half-sarcomeres from the Z-disk to the M-line (Furst et al., 1988; Itoh et al., 1988; Linke et al., 1997; Wang et al., 1991). Recently, it has been

suggested that titin has tunable stiffness depending on activation (Dutta et al., 2018; Granzier and Labeit, 2006; Labeit et al., 2003). Considering the in-parallel connection between titin and cross bridges (Herzog, 2018; Nishikawa, 2016; Trombitás and Granzier, 1997; Trombitás and Pollack, 1993), the tunable titin stiffness would have a significant impact on muscle stiffness.

In order to infer how titin stiffness is modulated by length history, muscle force and stiffness were measured during isometric force redevelopment following active shortening at different velocities. The y-intercept of the relationship between force and stiffness increased with decreasing shortening velocity, and the slope decreased with decreasing shortening velocity. Several of these findings are not easily explained by the traditional cross-bridge theory. Although non-constant ratio of force to stiffness can be explained by weakly-bound cross bridges, the lower slope with decreasing shortening velocity does not follow the cross-bridge theory. It has been hypothesized that actin distortion is responsible for depression of force after shortening, and that the amount of actin distortion is related to work or stress during active shortening (Joumaa et al., 2012; Maréchal and Plaghki, 1979). The slower shortening velocity would therefore cause a larger proportion of weakly-bound to strongly-bound cross bridges. The larger proportion of weakly- to strongly-bound cross bridges must produce the greater slope. However, we observed that the slower velocity yielded the lower slope.

To explain our findings, an additional tunable elastic element is required. The winding filament hypothesis developed by Nishikawa et al. (2012) suggests that the longitudinal rotation of actin changes titin stiffness by winding titin onto actin during the development of cross-bridge force. From variable y-intercepts in the relationship between force and stiffness, it can be speculated that active shortening sets the initial stiffness depending on shortening velocity. The winding filament hypothesis predicts that titin behavior during force development

should depend on the initial conditions, which results in different slopes in the relationship between force and stiffness.

5.3 Specific Aim 3: New muscle model including tunable stiffness.

One limitation of traditional Hill-type muscle models, is that they do not predict muscle force accurately under dynamic conditions due to the absence of history-dependent forces (Perreault et al., 2003; Sandercock and Heckman, 1997). To tackle this limitation, our new muscle model has added a titin element. A pulley representing thin filaments was also added between the contractile and titin elements to represent titin-actin interactions (Tahir et al., 2018). The history-dependent pulley position should affect the response of the model to activation, which allows for predicting history-dependent forces. Our results showed that the model with a pulley predicted frequency-dependent muscle forces better than the Hill model. This result demonstrates that adding a tunable titin element and titin-actin interactions improves force predictions during dynamic length changes.

5.4 Conclusion

This study addresses limitations of the current paradigm of muscle as motor and suggests an alternative viewpoint of muscle as active composite material. Muscle models based on the conventional viewpoint fail to capture the quick response of muscle to unpredicted perturbations and rapid velocity transients (Dick et al., 2017; Lee et al., 2013; Perreault et al., 2003; Sandercock and Heckman, 1997; Scovil and Ronsky, 2006). This study demonstrated that length history has a crucial role in determining muscle force. Muscle responds to activation and length perturbations depending on the mechanical properties determined by length history. In addition, this study investigated whether additional sarcomeric elements such as titin

contribute to the mechanical properties of muscle depending on length history. Length history affects the initial stiffness and strain of titin, which then would determine titin behavior in the active state. Based on the results of the investigations, this study proposes to define a new viewpoint of muscle as active composite material which can reflect the tunable elasticity of muscle based on the results of the proposed investigation. The muscle model developed in the active composite material viewpoint predicted muscle force under dynamic conditions more accurately than the Hill model based on the traditional viewpoint. Because muscle is the only tissue that produces active force, a predictive model of muscle force informs the understanding about how movement of the human body is controlled. This study anticipates that this new viewpoint of muscle research will inform applications including design and control principles for EMG-driven exo-skeletons and robotic prosthetics.

References

Abbott, B. C. and Aubert, X. M. (1952). The force exerted by active striated muscle during and after change of length. *J. Physiol.* **117**, 77–86.

Ahn, A. N., Meijer, K. and Full, R. J. (2006). In situ muscle power differs without varying in vitro mechanical properties in two insect leg muscles innervated by the same motor neuron. *J. Exp. Biol.* **209**, 3370–3382.

Alkner, B. A., Tesch, P. A. and Berg, H. E. (2000). Quadriceps EMG/force relationship in knee extension and leg press. *Med. Sci. Sports Exerc.* **32**, 459–463.

Brenner, B. and Eisenberg, E. (1986). Rate of force generation in muscle: Correlation with actomyosin ATPase activity in solution. *Proc. Natl. Acad. Sci. U. S. A.* **83**, 3542–3546.

Brunello, E., Caremani, M., Melli, L., Linari, M., Fernandez-Martinez, M., Narayanan, T., Irving, M., Piazzesi, G., Lombardi, V. and Reconditi, M. (2014). The contributions of filaments and cross-bridges to sarcomere compliance in skeletal muscle. *J. Physiol.* **592**, 3881–3899.

Buchanan, T. S., Lloyd, D. G., Manal, K. and Besier, T. F. (2004). Neuromusculoskeletal modeling: Estimation of muscle forces and joint moments and movements from measurements of neural command. *J. Appl. Biomech.*

Bullimore, S. R., Leonard, T. R., Rassier, D. E. and Herzog, W. (2007). History-dependence of isometric muscle force: effect of prior stretch or shortening amplitude. *J. Biomech.* **40**, 1518–1524.

Chow, J. W. and Darling, W. G. (1999). The maximum shortening velocity of muscle should be scaled with activation Differential adaptations to eccentric versus conventional resistance training in older humans The maximum shortening velocity of muscle should be scaled with activation. *J. Appl. Physiol.* **86**, 1025–1031.

Claflin, D. R. and Faulkner, J. A. (1989). The force-velocity relationship at high shortening velocities in the soleus muscle of the rat. *J. Physiol.* **411**, 627–637.

Cook, C. S. and McDonagh, M. J. (1995). Force responses to controlled stretches of electrically stimulated human muscle-tendon complex. *Exp. Physiol.* **80**, 477–490.

Daley, M. A. (2018). Understanding the Agility of Running Birds: Sensorimotor and Mechanical Factors in Avian Bipedal Locomotion. *Integr. Comp. Biol.* **58**, 884–893.

Daley, M. A. and Biewener, A. A. (2003). Muscle force-length dynamics during level versus incline locomotion: a comparison of in vivo performance of two guinea fowl ankle extensors. *J. Exp. Biol.* **206**, 2941–2958.

Daley, M. and Biewener, A. (2011). Leg muscles that mediate stability: Mechanics and control of two distal extensor muscles during obstacle negotiation in the guinea fowl. *Philos. Trans. R. Soc. B Biol. Sci.* **366**, 1580–1591.

Daley, M., Voloshina, A. and Biewener, A. (2009). The role of intrinsic muscle mechanics in the neuromuscular control of stable running in the guinea fowl. *J. Physiol.* **587**, 2693–2707.

Davies, R. E., Kushmerick, M. J. and Larson, R. E. (1967). ATP, activation, and the heat of shortening of muscle. *Nature* **214**, 148–151.

De Ruiter, C. J., De Haan, A., Jones, D. A. and Sargeant, A. J. (1998). Shortening-

induced force depression in human adductor pollicis muscle. *J. Physiol.* **507 (Pt 2**, 583–591.

Delp, S. L., Anderson, F. C., Arnold, A. S., Loan, P., Habib, A., John, C. T., Guendelman, E. and Thelen, D. G. (2007). OpenSim: Open-source software to create and analyze dynamic simulations of movement. *IEEE Trans. Biomed. Eng.* **54**, 1940–1950.

Dick, T. J. M., Arnold, A. S. and Wakeling, J. M. (2016). Quantifying Achilles tendon force in vivo from ultrasound images. *J. Biomech.* **49**, 3200–3207.

Dick, T. J. M., Biewener, A. A. and Wakeling, J. M. (2017). Comparison of human gastrocnemius forces predicted by Hill-type muscle models and estimated from ultrasound images. *J. Exp. Biol.* **220**, 1643–1653.

Dickinson, M. H., Farley, C. T., Full, R. J., Koehl, M. A., Kram, R. and Lehman, S. (2000). How animals move: an integrative view. *Science* **288**, 100–106.

Dominguez, R., Freyzon, Y., Trybus, K. M. and Cohen, C. (1998). Crystal structure of a vertebrate smooth muscle myosin motor domain and its complex with the essential light chain: visualization of the pre-power stroke state. *Cell* **94**, 559–571.

Dudek, D. M. and Full, R. J. (2006). Passive mechanical properties of legs from running insects. *J. Exp. Biol.* **209**, 1502–1515.

Dutta, S., Tsiros, C., Sundar, S. L., Athar, H., Moore, J., Nelson, B., Gage, M. J. and Nishikawa, K. (2018). Calcium increases titin N2A binding to F-actin and regulated thin filaments. *Sci. Rep.* **8**, 1–11.

Edman, K. A., Elzinga, G. and Noble, M. I. (1978). Enhancement of mechanical performance by stretch during tetanic contractions of vertebrate skeletal muscle fibres. *J. Physiol.* **281**, 139–155.

Edman, K. A., Elzinga, G. and Noble, M. I. (1982). Residual force enhancement after stretch of contracting frog single muscle fibers. *J. Gen. Physiol.* **80**, 769–784.

Finni, T., Komi, P. V. and Lukkariniemi, J. (1998). Achilles tendon loading during walking: Application of a novel optic fiber technique. *Eur. J. Appl. Physiol. Occup. Physiol.*

Ford, L. E., Huxley, A. F. and Simmons, R. M. (1981). The relation between stiffness and filament overlap in stimulated frog muscle fibres. *J. Physiol.* **311**, 219–249.

Forrester, S. E., Yeadon, M. R., King, M. A. and Pain, M. T. G. (2011). Comparing different approaches for determining joint torque parameters from isovelocity dynamometer measurements. *J. Biomech.* **44**, 955–961.

Full, R. J., Stokes, D. R., Ahn, A. N. and Josephson, R. K. (1998). Energy absorption during running by leg muscles in a cockroach. *J. Exp. Biol.* **201**, 997–1012.

Furst, D. O., Osborn, M., Nave, R. and Weber, K. (1988). The organization of titin filaments in the half-sarcomere revealed by monoclonal antibodies in immunoelectron microscopy: A map of ten nonrepetitive epitopes starting at the Z line extends close to the M line. *J. Cell Biol.* **106**, 1563–1572.

Gautel, M. and Goulding, D. (1996). A molecular map of titin/connectin elasticity reveals two different mechanisms acting in series. *FEBS Lett.* **385**, 11–14.

Geeves, M. A. and Holmes, K. C. (2005). The molecular mechanism of muscle contraction. *Adv. Protein Chem.* **71**, 161–193.

Gerus, P., Rao, G. and Berton, E. (2012). Subject-specific tendon-aponeurosis definition in Hill-type model predicts higher muscle forces in dynamic tasks. *PLoS One* **7**, e44406.

Gerus, P., Rao, G. and Berton, E. (2015). Ultrasound-based subject-specific parameters improve fascicle behaviour estimation in Hill-type muscle model. *Comput. Methods Biomech. Biomed. Engin.* **18**, 116–123.
Gordon, A. M., Huxley, A. F. and Julian, F. J. (1966). The variation in isometric tension with sarcomere length in vertebrate muscle fibres. *J. Physiol.* **184**, 170–192.
Granzier, H. L. and Labeit, S. (2006). The giant muscle protein titin is an adjustable molecular spring. *Exerc. Sport Sci. Rev.* **34**, 50–53.
Hahs, D. W. and Stiles, R. N. (1989). Buckle muscle tension transducer: What does it measure? *J. Biomech.* **22**, 165–166.
Herzog, W. (2018). The multiple roles of titin in muscle contraction and force production. *Biophys. Rev.* **10**, 1187–1199.
Herzog, W. (2019). Passive Force Enhancement in Striated Muscle. *J. Appl. Physiol.* 1782–1789.
Herzog, W. and Leonard, T. R. (1997). Depression of cat soleus forces following isokinetic shortening. *J. Biomech.* **30**, 865–872.
Herzog, W. and Leonard, T. R. (2000). The history dependence of force production in mammalian skeletal muscle following stretch-shortening and shortening-stretch cycles. *J. Biomech.* **33**, 531–542.
Herzog, W. and Leonard, T. R. (2002). Force enhancement following stretching of skeletal muscle: a new mechanism. *J. Exp. Biol.* **205**, 1275–1283.
Herzog, W., Schappacher, G., DuVall, M., Leonard, T. R. and Herzog, J. A. (2016). Residual force enhancement following eccentric contractions: A new mechanism involving titin. *Physiology* **31**, 300–312.
Hessel, A. L., Joumaa, V., Eck, S., Herzog, W. and Nishikawa, K. C. (2019). Optimal length, calcium sensitivity and twitch characteristics of skeletal muscles from mdm mice with a deletion in N2A titin. *J. Exp. Biol.* **222**,.
Hill, A. V. (1938). The heat of shortening and the dynamic constants of muscle. 612–745.
Hisey, B., Leonard, T. R. and Herzog, W. (2009). Does residual force enhancement increase with increasing stretch magnitudes? *J. Biomech.* **42**, 1488–1492.
Hof, A. L. and van den Berg, J. (1977). Linearity between the weighted sum of the EMGs of the human triceps surae and the total torque. *J. Biomech.* **10**, 529–539.
Hof, A. L. and Van den Berg, J. (1981). EMG to force processing I: An electrical analogue of the Hill muscle model. *J. Biomech.* **14**, 747–758.
Horowits, R. and Podolsky, R. J. (1987). The positional stability of thick filaments in activated skeletal muscle depends on sarcomere length: evidence for the role of titin filaments. *J. Cell Biol.* **105**, 2217–2223.
Hug, F., Hodges, P. W. and Tucker, K. (2015). Muscle Force Cannot Be Directly Inferred From Muscle Activation: Illustrated by the Proposed Imbalance of Force Between the Vastus Medialis and Vastus Lateralis in People With Patellofemoral Pain. *J. Orthop. Sport. Phys. Ther.* **45**, 360–365.
Huxley, A. F. (1957). Muscle structure and theories of contraction. *Prog. Biophys. Biophys. Chem.* 468.
Huxley, A. F. and Niedergerke, R. (1954). Structural changes in muscle during contraction: Interference microscopy of living muscle fibres. *Nature*.
Huxley, A. F. and Simmons, R. M. (1971). Proposed mechanism of force generation in striated muscle. *Nature* **233**, 533–538.

Hylander, W. L. and Johnson, K. R. (1989). The relationship between masseter force and masseter electromyogram during mastication in the monkey Macaca fascicularis. *Arch. Oral Biol.* **34**, 713–722.

Inman, V. T., Ralston, H. J., Saunders, J. B., Feinstein, B. and Wright, E. W. J. (1952). Relation of human electromyogram to muscular tension. *Electroencephalogr. Clin. Neurophysiol.* **4**, 187–194.

Itoh, Y., Suzuki, T., Kimura, S., Ohashi, K., Higuchi, H., Sawada, H., Shimizu, T., Shibata, M. and Maruyama, K. (1988). Extensible and less-extensible domains of connectin filaments in stretched vertebrate skeletal muscle sarcomeres as detected by immunofluorescence and immunoelectron microscopy using monoclonal antibodies. *J. Biochem.* **104**, 504–508.

James, R. and Johnston, I. (1998). Scaling of muscle performance during escape responses in the fish myoxocephalus scorpius L. *J. Exp. Biol.* **201 (Pt 7)**, 913–923.

Johnston, K., Jinha, A. and Herzog, W. (2016). The role of sarcomere length non-uniformities in residual force enhancement of skeletal muscle myofibrils. *R. Soc. open Sci.* **3**, 150657.

Jones, A. A., Power, G. A. and Herzog, W. (2016). History dependence of the electromyogram: Implications for isometric steady-state EMG parameters following a lengthening or shortening contraction. *J. Electromyogr. Kinesiol.* **27**, 30–38.

Joumaa, V., MacIntosh, B. R. and Herzog, W. (2012). New insights into force depression in skeletal muscle. *J. Exp. Biol.* **215**, 2135–2140.

Julian, F. J. and Morgan, D. L. (1981). Variation of muscle stiffness with tension during tension transients and constant velocity shortening in the frog. *J. Physiol.* **319**, 193–203.

Julian, F. J. and Sollins, M. R. (1975). Variation of muscle stiffness with force at increasing speeds of shortening. *J. Gen. Physiol.* **66**, 287–302.

Kirsch, R. F., Boskov, D. and Rymer, W. Z. (1994). Muscle stiffness during transient and continuous movements of cat muscle: perturbation characteristics and physiological relevance. *IEEE Trans. Biomed. Eng.* **41**, 758–770.

Kuo, A. D. (1998). A least-squares estimation approach to improving the precision of inverse dynamics computations. *J. Biomech. Eng.* **120**, 148–159.

Labeit, D., Watanabe, K., Witt, C., Fujita, H., Wu, Y., Lahmers, S., Funck, T., Labeit, S. and Granzier, H. (2003). Calcium-dependent molecular spring elements in the giant protein titin. *Proc. Natl. Acad. Sci. U. S. A.* **100**, 13716–13721.

Lappin, A. K., Monroy, J. A., Pilarski, J. Q., Zepnewski, E. D., Pierotti, D. J. and Nishikawa, K. C. (2006). Storage and recovery of elastic potential energy powers ballistic prey capture in toads. *J. Exp. Biol.* **209**, 2535–2553.

Lee, H.-D. and Herzog, W. (2002). Force enhancement following muscle stretch of electrically stimulated and voluntarily activated human adductor pollicis. *J. Physiol.* **545**, 321–330.

Lee, H. D. and Herzog, W. (2003). Force depression following muscle shortening of voluntarily activated and electrically stimulated human adductor pollicis. *J. Physiol.* **551**, 993–1003.

Lee, E.-J. and Herzog, W. (2008). Residual force enhancement exceeds the isometric force at optimal sarcomere length for optimized stretch conditions. *J. Appl. Physiol.* **105**, 457–462.

Lee, E.-J. and Herzog, W. (2009). Shortening-induced force depression is primarily caused

by cross-bridges in strongly bound states. *J. Biomech.* **42**, 2336–2340.
Lee, S. S. M., Arnold, A. S., Miara, M. de B., Biewener, A. A. and Wakeling, J. M. (2013). Accuracy of gastrocnemius muscles forces in walking and running goats predicted by one-element and two-element Hill-type models. *J. Biomech.* **46**, 2288–2295.
Leonard, T. R. and Herzog, W. (2005). Does the speed of shortening affect steady-state force depression in cat soleus muscle? *J. Biomech.* **38**, 2190–2197.
Leonard, T. R., DuVall, M. and Herzog, W. (2010). Force enhancement following stretch in a single sarcomere. *Am. J. Physiol. Cell Physiol.* **299**, C1398-401.
Li, Q., Jin, J. P. and Granzier, H. L. (1995). The effect of genetically expressed cardiac titin fragments on in vitro actin motility. *Biophys. J.* **69**, 1508–1518.
Libby, T., Chukwueke, C. and Sponberg, S. (2020). History-dependent perturbation response in limb muscle. *J. Exp. Biol.* **223**, 509646.
Lindstedt, S. and Nishikawa, K. (2017). *Huxleys' Missing Filament: Form and Function of Titin in Vertebrate Striated Muscle*.
Linke, W. A., Ivemeyer, M., Labeit, S., Hinssen, H., Rüegg, J. C. and Gautel, M. (1997). Actin-titin interaction in cardiac myofibrils: Probing a physiological role. *Biophys. J.* **73**, 905–919.
Linke, W. A., Stockmeier, M. R., Ivemeyer, M., Hosser, H. and Mundel, P. (1998a). Characterizing titin's I-band Ig domain region as an entropic spring. *J. Cell Sci.* **111**, 1567–1574.
Linke, W. A., Ivemeyer, M., Mundel, P., Stockmeier, M. R. and Kolmerer, B. (1998b). Nature of PEVK-titin elasticity in skeletal muscle. *Proc. Natl. Acad. Sci. U. S. A.* **95**, 8052–8057.
Lloyd, D. G. and Besier, T. F. (2003). An EMG-driven musculoskeletal model to estimate muscle forces and knee joint moments in vivo. *J. Biomech.* **36**, 765–776.
Lymn, R. W. and Taylor, E. W. (1971). Mechanism of adenosine triphosphate hydrolysis by actomyosin. *Biochemistry* **10**, 4617–4624.
Maganaris, C. N. and Paul, J. P. (1999). In vivo human tendon mechanical properties. *J. Physiol.* **521**, 307–313.
Maréchal, G. and Plaghki, L. (1979). The deficit of the isometric tetanic tension redeveloped after a release of frog muscle at a constant velocity. *J. Gen. Physiol.* **73**, 453–467.
Maruyama, K., Sawada, H., Kimura, S., Ohashi, K., Higuchi, H. and Umazume, Y. (1984). Connectin filaments in stretched skinned fibers of frog skeletal muscle. *J. Cell Biol.* **99**, 1391–1397.
Monroy, J. A., Powers, K. L., Pace, C. M., Uyeno, T. and Nishikawa, K. C. (2017). Effects of activation on the elastic properties of intact soleus muscles with a deletion in titin. *J. Exp. Biol.* **220**, 828–836.
Morgan, D. L. (1990). New insights into the behavior of muscle during active lengthening. *Biophys. J.* **57**, 209–221.
Morgan, D. L., Whitehead, N. P., Wise, A. K., Gregory, J. E. and Proske, U. (2000). Tension changes in the cat soleus muscle following slow stretch or shortening of the contracting muscle. *J. Physiol.* **522 Pt 3**, 503–513.
Nishikawa, K. C. (2016). Eccentric contraction: Unraveling mechanisms of force enhancement and energy conservation. *J. Exp. Biol.* **219**, 189–196.

Nishikawa, K. C. (2020). Titin: A tunable spring in active muscle. *Physiology* **35**, 209–217.
Nishikawa, K., Biewener, A. A., Aerts, P., Ahn, A. N., Chiel, H. J., Daley, M. A., Daniel, T. L., Full, R. J., Hale, M. E., Hedrick, T. L., et al. (2007). Neuromechanics: an integrative approach for understanding motor control. *Integr. Comp. Biol.* **47**, 16–54.
Nishikawa, K. C., Monroy, J. A. J. A., Uyeno, T. E., Yeo, S. H. S. H., Pai, D. K. D. K. and Lindstedt, S. L. S. L. (2012). Is titin a "winding filament"? A new twist on muscle contraction. *Proc. R. Soc. B Biol. Sci.* **279**, 981–990.
Nishikawa, K. C., Monroy, J. A., Powers, K. L., Gilmore, L. A., Uyeno, T. A. and Lindstedt, S. L. (2013). *A molecular basis for intrinsic muscle properties: Implications for motor control*.
Oda, T. and Yanagisawa, H. (2020). Cryo-electron tomography of cardiac myofibrils reveals a 3D lattice spring within the Z-discs. *Commun. Biol.* **3**, 1–9.
Olney, S. J. and Winter, D. A. (1985). Predictions of knee and ankle moments of force in walking from EMG and kinematic data. *J. Biomech.* **18**, 9–20.
Perreault, E. J., Heckman, C. J. and Sandercock, T. G. (2003). Hill muscle model errors during movement are greatest within the physiologically relevant range of motor unit firing rates. *J. Biomech.* **36**, 211–218.
Peterson, D. R., Rassier, D. E. and Herzog, W. (2004). Force enhancement in single skeletal muscle fibres on the ascending limb of the force-length relationship. *J. Exp. Biol.* **207**, 2787–2791.
Pun, C., Syed, A. and Rassier, D. E. (2010). History-dependent properties of skeletal muscle myofibrils contracting along the ascending limb of the force-length relationship. *Proceedings. Biol. Sci.* **277**, 475–484.
Rassier, D. E. and Herzog, W. (2004). Effects of shortening on stretch-induced force enhancement in single skeletal muscle fibers. *J. Biomech.* **37**, 1305–1312.
Rassier, D. E., Herzog, W., Wakeling, J. and Syme, D. A. (2003). Stretch-induced, steady-state force enhancement in single skeletal muscle fibers exceeds the isometric force at optimum fiber length. *J. Biomech.* **36**, 1309–1316.
Rayment, I., Holden, H. M., Whittaker, M., Yohn, C. B., Lorenz, M., Holmes, K. C. and Milligan, R. A. (1993). Structure of the actin-myosin complex and its implications for muscle contraction. *Science* **261**, 58–65.
Roberts, T. J., Marsh, R. L., Weyand, P. G. and Taylor, C. R. (1997). Muscular force in running turkeys: the economy of minimizing work. *Science* **275**, 1113–1115.
Robertson, B. D. and Sawicki, G. S. (2015). Unconstrained muscle-tendon workloops indicate resonance tuning as a mechanism for elastic limb behavior during terrestrial locomotion. *Proc. Natl. Acad. Sci. U. S. A.* **112**, E5891–E5898.
Sandercock, T. G. and Heckman, C. J. J. (1997). Force from cat soleus muscle during imposed locomotor-like movements: Experimental data versus Hill-type model predictions. *J. Neurophysiol.* **77**, 1538–1552.
Scovil, C. Y. and Ronsky, J. L. (2006). Sensitivity of a Hill-based muscle model to perturbations in model parameters. *J. Biomech.* **39**, 2055–2063.
Seiberl, W., Paternoster, F., Achatz, F., Schwirtz, A. and Hahn, D. (2013). On the relevance of residual force enhancement for everyday human movement. *J. Biomech.* **46**, 1996–2001.
Seth, A., Sherman, M., Reinbolt, J. A. J. A. and Delp, S. L. S. L. (2011). OpenSim: A musculoskeletal modeling and simulation framework for in silico investigations and

exchange. *Procedia IUTAM* **2**, 212–232.
Seyfert, S. and Künkel, H. (1974). Analysis of muscular activity during voluntary contraction of different strengths. *Electromyogr. Clin. Neurophysiol.* **14**, 323–330.
Shalabi, N., Cornachione, A., de Souza Leite, F., Vengallatore, S. and Rassier, D. E. (2017). Residual force enhancement is regulated by titin in skeletal and cardiac myofibrils. *J. Physiol.* **595**, 2085–2098.
Shue, G.-H. and Crago, P. E. (1998). Muscle-tendon model with length history-dependent activation-velocity coupling. *Ann. Biomed. Eng.* **26**, 369–380.
Smith, T. G. and Stokes, M. J. (1993). Technical aspects of acoustic myography (AMG) of human skeletal muscle: contact pressure and force/AMG relationships. *J. Neurosci. Methods* **47**, 85–92.
Sponberg, S., Spence, A. J., Mullens, C. H. and Full, R. J. (2011a). A single muscle's multifunctional control potential of body dynamics for postural control and running. *Philos. Trans. R. Soc. B Biol. Sci.* **366**, 1592–1605.
Sponberg, S., Libby, T., Mullens, C. H. and Full, R. J. (2011b). Shifts in a single muscle's control potential of body dynamics are determined by mechanical feedback. *Philos. Trans. R. Soc. Lond. B. Biol. Sci.* **366**, 1606–1620.
Sugi, H. (1972). Tension changes during and after stretch in frog muscle fibres. *J. Physiol.* **225**, 237–253.
Sugi, H. and Tsuchiya, T. (1988). Stiffness changes during enhancement and deficit of isometric force by slow length changes in frog skeletal muscle fibres. *J. Physiol.* **407**, 215–229.
Tahir, U., Hessel, A. L., Lockwood, E. R., Tester, J. T., Han, Z., Rivera, D. J., Covey, K. L., Huck, T. G., Rice, N. A. and Nishikawa, K. C. (2018). Case study: A bio-inspired control algorithm for a robotic foot-ankle prosthesis provides adaptive control of level walking and stair ascent. *Front. Robot. AI* **5**,.
Tahir, U., Monroy, J. A., Rice, N. A. and Nishikawa, K. C. (2020). Effects of a titin mutation on force enhancement and force depression in mouse soleus muscles. *J. Exp. Biol.* **223**,.
Thelen, D. G. (2003). Adjustment of muscle mechanics model parameters to simulate dynamic contractions in older adults. *J. Biomech. Eng.* **125**, 70–77.
Trinick, J., Knight, P. and Whiting, A. (1984). Purification and properties of native titin. *J. Mol. Biol.* **180**, 331–356.
Trombitás, K. and Granzier, H. (1997). Actin removal from cardiac myocytes shows that near Z line titin attaches to actin while under tension. *Am. J. Physiol.* **273**, C662-70.
Trombitás, K. and Pollack, G. H. (1993). Elastic properties of the titin filament in the Z-line region of vertebrate striated muscle. *J. Muscle Res. Cell Motil.* **14**, 416–422.
van Ruijven, L. J. and Weijs, W. A. (1990). A new model for calculating muscle forces from electromyograms. *Eur. J. Appl. Physiol. Occup. Physiol.* **61**, 479–485.
Wakeling, J. M., Tijs, C., Konow, N. and Biewener, A. A. (2021). Modeling muscle function using experimentally determined subject-specific muscle properties. *J. Biomech.* **117**, 110242.
Wang, K., Ramirez-Mitchell, R. and Palter, D. (1984). Titin is an extraordinarily long, flexible, and slender myofibrillar protein. *Proc. Natl. Acad. Sci. U. S. A.* **81**, 3685–3689.
Wang, K., Mccarter, R., Wright, J., Beverly, J. and Ramirez-Mitchell, R. (1991). Regulation of skeletal muscle stiffness and elasticity by titin isoforms: A test of the

segmental extension model of resting tension. *Proc. Natl. Acad. Sci. U. S. A.* **88**, 7101–7105.

Wang, K., McCarter, R., Wright, J., Beverly, J. and Ramirez-Mitchell, R. (1993). Viscoelasticity of the sarcomere matrix of skeletal muscles. The titin-myosin composite filament is a dual-stage molecular spring. *Biophys. J.* **64**, 1161–1177.

Yeadon, M. R., King, M. A. and Wilson, C. (2006). Modelling the maximum voluntary joint torque/angular velocity relationship in human movement. *J. Biomech.* **39**, 476–482.

Zahalak, G. I. (1997). Can muscle fibers be stable on the descending limbs of their sarcomere length-tension relations? *J. Biomech.* **30**, 1179–1182.

Zajac, F. E. (1989). Muscle and tendon: properties, models, scaling, and application to biomechanics and motor control. *Crit. Rev. Biomed. Eng.* **17**, 359–411.